Chapter 2
Numerical Methods of Multifractal Analysis in Information Communication Systems and Networks

Oleg I. Sheluhin
Moscow Technical University of Communications and Informatics, Russia

Artem V. Garmashev
Moscow Technical University of Communications and Informatics, Russia

ABSTRACT

In this chapter, the main principles of the theory of fractals and multifractals are stated. A singularity spectrum is introduced for the random telecommunication traffic, concepts of fractal dimensions and scaling functions, and methods used in their determination by means of Wavelet Transform Modulus Maxima (WTMM) are proposed. Algorithm development methods for estimating multifractal spectrum are presented. A method based on multifractal data analysis at network layer level by means of WTMM is proposed for the detection of traffic anomalies in computer and telecommunication networks. The chapter also introduces WTMM as the informative indicator to exploit the distinction of fractal dimensions on various parts of a given dataset. A novel approach based on the use of multifractal spectrum parameters is proposed for estimating queuing performance for the generalized multifractal traffic on the input of a buffering device. It is shown that the multifractal character of traffic has significant impact on queuing performance characteristics.

INTRODUCTION

Often in telecommunication applications, the measured characteristics of traffic datasets display stochastic self-similar properties (i.e. *fractality*). Here it is assumed that a measure of similarity is the traffic type with appropriate amplitude normalization. Accurate structural observation is complicated for datasets, self-similarity however allows for considering the stochastic nature of many network devices and events, which jointly influence the network traffic. One value suffices

DOI: 10.4018/978-1-4666-2208-1.ch002

for the quantitative description of fractals (i.e. the *Hausdorff dimension* or a scaling index) describing an invariance of geometry or statistical performances at a given level of rescaling. However in the fields of physics, chemistry, biology, and telecommunications, there are many appearances, which demand propagation of the fractal concept on complicated structures with more than one scaling index. Such structures are often characterized by a whole spectrum of indices and *Hausdorff dimension* is only one of them. Complex fractals, also known as *multifractals,* are important because they as a rule occur in nature, whereas simple self-similar objects represent idealization of real appearances. Actually, employment of the multifractal approach means that the studied object somehow can be divided into parts, each having its own self-similar properties.

Thus multifractals are *non-homogeneous fractal* objects, for which complete description is required, unlike the regular fractals, there is not enough information in any one value of fractal dimension, but a whole spectrum of such dimensions is required, the number of which, generally speaking, is infinite. The distinctive feature of the latter consists in the fact that they, along with the global characteristics of stochastic processes (obtained as a result of the procedure of averaging on large time intervals), allow for considering singularities of their local structure. Their versatility is in important techniques based on fractal representations and wavelet transforms.

The material in this chapter is divided into three parts. The first part sets out the basic theory of fractals and multifractals, as well as methods of determining the basic parameters of multifractal processes using wavelet transforms. The other two parts deal with specific technical tasks, where investigation of multifractal properties of the processed sequences yield innovative solutions and algorithms. The second part is devoted to the use of fractal analysis for problems of detection of traffic anomaly, which allows for a fundamentally new approach to algorithms development. In the third part, for the generalized multifractal traffic the new practical evaluation method of telecommunication networks queuing performance is offered.

THEORY OF FRACTALS AND MULTIFRACTALS

The term "*fractal*" was used for the first time in Benoît Mandelbrot's work (Mandelbrot, 1982). The word fractal is derived from the Latin *fractus* meaning "fractured" or "broken." Mandelbrot used the term "fractals" for geometric objects that have strongly fragmented shape and can possess the property of *self-similarity*. It is possible to generalize the concept of fractal to any object (image, speech, telecommunication traffic, etc.) some parameters of which are remain invariant with change in scale or time. Thus, the principal property of such objects (i.e. self-similarity) implies that at augmentation, its parts are similar (in some specified sense) to its total shape.

The property of exact self-similarity is a characteristic of the regular fractals only. If an element of randomness is to be included in the algorithm of their creation instead of the determined method of construction (as it happens, for example, in many processes of diffusion growth of clusters, voltage failure, etc.), then the so-called incidental fractals appear. Their basic difference from regular ones is that the property of self-similarity holds true only after a corresponding averaging on the base of all statistically independent realizations of the object. For quantitative description of fractals, a single value is enough - a fractal dimension (Hausdorff dimension) or the index of scaling which is determined as follows

$$D_f = -\lim_{\varepsilon \to 0} \frac{lnM\left(\varepsilon\right)}{\ln\left(\frac{1}{\varepsilon}\right)} \qquad (1)$$

Here D_f is fractal dimension of set occupying area by volume of L^{D_f} in D-dimensional space, covered with a number of cubes with a volume of ε^{D_f}. The minimum number of such nonempty cubes occupying the set is $M\left(\varepsilon\right) = L^{D_f}\left(1/\varepsilon\right)^{D_f}$. Apart from regular fractals there is a special class of fractal objects, within which the distribution of points of set is heterogeneous. The reason of heterogeneity is different occupation probabilities of geometrically identical elements of the fractal, or in the general case, a disparity of occupation probabilities with geometrical sizes of the corresponding areas. Such heterogeneous fractal objects are known as multifractals. For their complete description, unlike the case of regular fractals introducing only one value, its fractal dimension D_f, is not enough, and the whole spectrum of such dimensions, infinite in their number, is required. It can be accounted for by the fact that such fractals also possess some statistical properties along with the purely geometrical descriptions determined by D_f dimension.

General definition of a multifractal: we consider a fractal object occupying a certain limited area L of the size L in Euclidean space with dimension d. We divide the whole area under L into cubic cells having a length of size $\varepsilon << L$ and a volume ε^d. We will hereafter be interested only in the occupied cells containing at least one point. Let the number of the occupied cells *i* change within the range of $1,2,\ldots,N(\varepsilon)$, where $N(\varepsilon)$ is the general number of the occupied cells, defined naturally, by the size of the cell ε. Let $n_i\left(\varepsilon\right)$ be the quantity of points in the i^{th} cell, then the value

$$p_i\left(\varepsilon\right) = \lim_{N\to\infty}\frac{n_i\left(\varepsilon\right)}{N} \tag{2}$$

represents the probability of a point taken at random from our set being in the cell *i*. In other words, probabilities *p*, characterize the relative filing of the cells. It follows from the normalizing condition of probability that

$$\sum_{i=1}^{N(\varepsilon)} p_i\left(\varepsilon\right) = 1 \tag{3}$$

We now consider the generalized statistical sum $S\left(q,\varepsilon\right)$ (henceforth called the *decomposition function*), characterized by an exponent *q*, which can take any values in the range of $-\infty < q < +\infty$

$$S\left(q,\varepsilon\right) = \sum_{i=1}^{N(\varepsilon)} p_i\left(\varepsilon\right) \tag{4}$$

The spectrum of generalized fractal dimensions D_q characterizing the given distribution of points in area L, is defined by the following correlation:

$$D_q = \frac{\tau\left(q\right)}{q-1} \tag{5}$$

where the function $\tau\left(q\right)$ is defined as

$$\tau\left(q\right) = \lim_{\varepsilon\to 0}\left(\frac{\ln S\left(q,\varepsilon\right)}{\ln\varepsilon}\right) \tag{6}$$

If $D_q = D = const$ (i.e. it does not depend on *q*) then the given set of points represents a regular fractal (*monofractal*), characterized only by one value – the fractal dimension D. On the contrary, if the function D_q somehow varies with change in q, then the considered set of points is a multifractal. Thus, the multifractal is generally characterized by some nonlinear function τ_q (hereafter called the scaling function) defining the behavior of the statistical sum $S\left(q,\varepsilon\right)$ at $\varepsilon \to 0$.

$$S\left(q,\varepsilon\right)=\sum_{i=1}^{N}p_i^q\left(\varepsilon\right)\approx\varepsilon^{\tau\left(q\right)} \tag{7}$$

Bozhokin and Parshin (2001) showed what physical meaning the spectrum of generalized fractal dimensions D_q has at various values of q. Thus, at *q=0*

$$N\left(\varepsilon\right)\approx\varepsilon^{-D_0} \tag{8}$$

It means that the value D_0 represents the usual *Hausdorff Dimension* of the set L. It is the roughest characteristic of a multifractal and does not provide any information on its statistical properties.

At *q=1*

$$D_1=-\lim_{\varepsilon\to 0}\frac{Z\left(\varepsilon\right)}{\ln\varepsilon} \tag{9}$$

where $Z\left(\varepsilon\right)=-\sum_{i=1}^{N\left(\varepsilon\right)}p_i\ln p_i$ represents the entropy of a fractal set.

This definition of the entropy of a set is completely identical to the one used in thermodynamics where p_i is the probability of detecting a system in a quantum condition *i*. *Claude E. Shannon* generalized the concept of entropy *Z* known in thermodynamics, in his epochal work on the mathematical theory of communication (Shannon, 1948). For such problems, entropy became a measure of the information quantity required for defining a system in some position *i*. In other words, it is *a measure of our ignorance of the system*, i.e. a measure of uncertainty about the system. Coming back to initial problem of distribution of points in the fractal set L, it is possible to say, that since from (9) it follows that

$$Z\left(\varepsilon\right)\approx\varepsilon^{-D_1} \tag{10}$$

then the value D_1 characterizes the information necessary for the definition of the location of a point in some cell. This is why the generalized fractal dimension D_1 is often called *information dimension*. It shows how the information necessary for the definition of location of a point increases when the size of the cell ε tends to zero.

At $q=2,$ we have

$$D_2=\lim_{\varepsilon\to 0}\frac{\sum_{i=1}^{N\left(\varepsilon\right)}p_i^2}{\ln\varepsilon} \tag{11}$$

the paired correlation integral is defined as

$$I\left(\varepsilon\right)=\lim_{N\to\infty}\frac{1}{N^2}\sum_{n,m}\theta\left(\varepsilon-\left|r_n-r_m\right|\right) \tag{12}$$

where summation is done for all pairs of points in our fractal set with radius-vectors r_n and r_m; $\theta\left(x\right)-$ is the Heaviside's step function. $\theta\left(x\right)=1,$ if $x\geq 0$ and $\theta\left(x\right)=0,$ if $x<0.$

The sum in the expression (12) defines the number of pairs of points *n, m*, with the distance between them less than ε. Divided by N^2, it defines the probability of two randomly chosen points to be separated by a distance smaller than ε[12]. The same probability can be defined in another way. The value $p_i,$ according to its definition in (2), represents the probability of a point being in the cell *i* having size ε. Hence, the value p_i can be defined as the probability of two points being in this cell. By finding the sum of p_i^2 for all occupied cells, we will get the probability of any two randomly chosen points from set L falling in a cell with size ε. Consequently, the distance between these points will be less than or of an order of ε. Thus taking Equation (11) into consideration, we have

$$I\left(\varepsilon\right) \approx \sum_{i=1}^{N(\varepsilon)} p_i^2 \approx \varepsilon^{D_2} \tag{13}$$

It is possible to draw the conclusion that the generalized dimension D_2 defines the dependence of the correlation integral $I\left(\varepsilon\right)$ on ε. It is for this reason that the value D_2 is known as the correlation dimension. However, the values of D_q are not, strictly speaking, fractal dimensions in the generally accepted sense. Therefore, along with them, the so-called function of multifractal spectrum (multifractal singularities spectrum) is often used to characterize the multifractal set. One of the main characteristics of a multifractal is a set of probabilities p_i, showing the relative filling of cells ε, covering the set. The smaller the cell is, the smaller its filling. For self-similar sets, the dependence of p_i, on the size of the cell has an exponential character

$$p_i\left(\varepsilon\right) \approx \varepsilon^{\alpha_i} \tag{14}$$

where α_i is some exponent (different for different cells *i*).

Let $n\left(\alpha\right)d\alpha$ be the probability of α_i being in a range from $\alpha to d\alpha$. In other words, $n\left(\alpha\right)d\alpha$ represents the relative number of cells *i*, with the same measure of p_i with α_i, lying in this range. In the case of a monofractals, for which all α_i are the same (and equal to the fractal dimension *D*), this number is obviously proportional to the total number of cells $N\left(\varepsilon\right) \approx \varepsilon^{-D}$, dependent by extension on the size of the cell ε. The fractal dimension of the set D determines the index in this ratio. However, it is not accurately true for multifractals, and different values of α_i occur with a probability that is characterized not by one and the same value of *D*, but by different values (according to α) of the exponent $f\left(\alpha\right)$,

$$n\left(\alpha\right) \approx \varepsilon^{-f(\alpha)} \tag{15}$$

Thus the physical meaning of the function $f\left(\alpha\right)$ is that it represents the Hausdorff dimension of a homogeneous fractal subset L_α, from the original set L, characterized by equal probabilities of filling of the cells $p_i \approx \varepsilon$. Since the fractal dimension of a subset is clearly always less than or equal to the fractal dimension of the original set D_0, there is an important inequality for the function $f\left(\alpha\right)$:

$$f\left(\alpha\right) \le D_0 \tag{16}$$

The conclusion is that a set of different values of the function $f\left(\alpha\right)$ (for different α) represents a spectrum of fractal dimensions of homogeneous subsets of L_α into which the original set of L can be divided. This explains the term of a multifractal. It can be understood as a kind of incorporation of the various homogeneous fractal subsets L_α of the original set of L, each of which has its own value of the fractal dimension $f\left(\alpha\right)$. Since any subset contains only a fraction of the total number of cells $N\left(\varepsilon\right)$, into which the initial set of L is divided, normalization condition of probability (3), is obviously not fulfilled in the case of summation for this subset only. Since the sum of the probabilities is less than one. Therefore, the probabilities p_i with the same value of α_i are obviously less than or at least are of the same order as the value $\varepsilon^{f(\alpha_i)}$, which is inversely proportional to the number of cells, covering the given subset (in the case of a monofractal

decompose input signal $s(t)$ into its coefficients:

$$W_s(u,j) = (s(t), \psi_{u,j}(t)) = 2^{-j/2} \int_{-\infty}^{\infty} s(t)\psi\left(\frac{t-u}{2^j}\right)dt,$$

Step 2: In the resulting array of wavelet coefficients, find the position of local maxima and their absolute values $\left\{u_p(j)\right\}_{p\in Z}$, thus forming an array of local maxima $\left|W_s(u_p, j)\right|$

Step 3: Calculate the partition function:

$$S(q,j) = \sum_P \left|W_s(u_p, j)\right|^q$$

Step 4: Calculate the scaling function $\tau(q)$ for each $q \in R$:

$$\tau(q,j) = \liminf_{j\to 0} \frac{\ln S(q,j)}{\ln 2^j}$$

Step 5: Using the Legendre transform, compute the multifractal spectrum $f_L(\alpha)$

$$f_L(\alpha, j) = \min_{q\in R}(q(\alpha) - \tau(q,j))$$

Step 6: For each octave *j*, compute multifractal dimension of order *q*:

$$D_{q,j} = \frac{1}{q-1}[q(\alpha(q,j) - f(\alpha(q), j)]$$

For $q < 0$ the value of $S(q,j)$ depends mainly on small maxima of the amplitude $\left|Wf(u_p, j)\right|$. It is for this reason that the computation maybe unstable. To avoid false modulus-maxima created by computational errors in areas where *s* is almost constant, wavelet-maxima are chained together to form a scale-dependent curve of maxima.

If $\psi = (-1)^P \theta^{(p)}$, where $\theta = \frac{1}{\sqrt{2\pi}} e^{=t^2/2}$ is the Gaussian function, then all the lines of maxima $u_p(j)$ define curves that spread up to the limit $j=0$. Therefore, all maxima lines, that do not spread up to the smallest scale are removed in the calculation of $S(q,j)$.

MULTIFRACTAL ANALYSIS IN THE DETECTION OF TELECOMMUNICATION TRAFFIC ANOMALIES

Researches (Sheluhin, Smolskiy, & Osin, 2007; Bacry, Muzy, & Arneodo, 1993; Jaffard, 1997; Riedi, Crouse, Ribeiro, & Baraniuk, 1997; Meyer, 1997; Feldmann, Gilbert, & Willinger, 1998) abound which show that the network traffic is self-similar in time scales of the order of some hundreds of milliseconds and more. At the same time, it also shows multifractal properties in smaller time scales (the order of milliseconds). It is possible to tell that self-similarity reflects long-range behavior of a measured signal, and multifractal properties reflect its instant behavior. The search for singularity distribution (peculiarity) in a multifractal signal is very important for the analysis of its properties. A number of methods have been advanced in the literature for the determination of the singularity spectrum of a multifractal signal based on wavelet transform (Riedi, Crouse, Ribeiro, & Baraniuk, 1999 ; Muzy, Bacry, & Arneodo, 1999).

Datasets made available by the Lincoln Laboratory of MIT - 1999 DARPA Intrusion Detection Evaluation (MIT, 2012) were analyzed as the experimental test sequence. The datasets are network traffic collected by the end router of the institute's network. Figure 5a shows a realization of pure network traffic without attack for 72,700 s (~20 hours) sampled at 1s intervals, while Figure 5b depicts the same realization with different types of anomalies relating to attacks such as Denial of

sequence of modulus-maxima that converges to ν on small scales (Hwang and Mallat, 1994). For this reason, a set of maxima of scale *j* may be interpreted as covering the carrier of the singularity *s* with wavelets of scale 2^j at the points of occurrence of these maxima.

$$\left|W_s(u,j)\right| \sim 2^{j(\alpha_0+1/2)} \tag{25}$$

Let $\left\{u_p(j)\right\}_{p\in Z}$ – be the position of local maxima of $\left|W_s(u,j)\right|$ on a fixed scale *j*. Partition function *S* measures the sum of all these maxima of wavelet-modulus raised to power *q*:

$$S(q,j) = \sum_P \left|W_s(u_p,j)\right|^q \tag{26}$$

For each scale *s*, it is assumed that any two consecutive maxima u_p and u_{p+1} are located at distance $|u_{p+1}-u_p| > \varepsilon s$ for a given $\varepsilon > 0$. If this is not so then at intervals with size $\varepsilon 2^j$, the sum expressed in (26) will consist of only the maxima with the highest amplitudes. This concept protects the partition function from superposition of close maxima that are consequences of fast oscillations. For each $q \in R$, the scaling function $\tau(q)$ measures the asymptotic decrease of $S(q,j)$ at small scales of *j*:

$$\tau(q,j) = \liminf_{j\to 0} \frac{\ln S(q,j)}{\ln 2^j} \tag{27}$$

This usually implies that $S(q,j) \sim 2^{j\tau(q)}$.

Function $\tau(q)$ is connected to the Legendre transform for self-similar signals through expression (28). This result has been discovered (Bacry, Muzy, Arneodo, 1993) for a private class of fractal signals and generalized by Zhaffar (1997).

$$\tau(q,j) = \min_{\alpha\in\wedge}(q(\alpha) - f_L(\alpha,J)) \tag{28}$$

This theorem proves that the scaling function $\tau(q)$ is the Legendre transform of function $f_L(\alpha)$. For this purpose it is necessary to use only wavelet with a sufficient number of zero moments. At numerical implementations $\tau(q)$ is estimated via the evaluation of $S(q,\varepsilon)$. Therefore it is necessary to convert the Legendre transform in (28) to recover a singularity spectrum $f_L(\alpha)$.

It can be shown that the scaling function $\tau(q)$ is a convex and increasing function of *q* (Mallat, 2005) that the spectrum $f(\alpha)$ of the self-similar signals is convex, while the Legendre transform in Equation (28) is reversible *iff* $f(\alpha)$ is a convex function. In this case Equation (29) holds.

$$f_L(\alpha,j) = \min_{q\in R}(q(\alpha) - \tau(q,j)) \tag{29}$$

This formula holds for a wide class of multifractals. For example, it may be applied in the case of statistical self-similar signals such as in the realization of Fractional Brownian Motion (FBM). The multifractals having some stochastic self-similarity have a spectrum, which can be often calculated as reversal of Legendre transform (29). However, we pay special attention that this formula is not exact for any function *s*, because its spectrum of singularities $f_L(\alpha)$ is not mandatorily convex. Generally, it was proved in (Zhaffar, 1997) that Legendre transform (28) gives only upper bound of $f_L(\alpha)$.

WTMM ALGORITHM FOR ESTIMATING MULTIFRACTAL SPECTRAL PARAMETERS

Algorithm of the method applied in the estimation of multifractal spectral parameters is presented below.

Step 1: With the aid of continuous dyadic wavelet-transform of the mother wavelet $\psi(t)$,

Figure 4. Singularity spectrum of the multifractal process

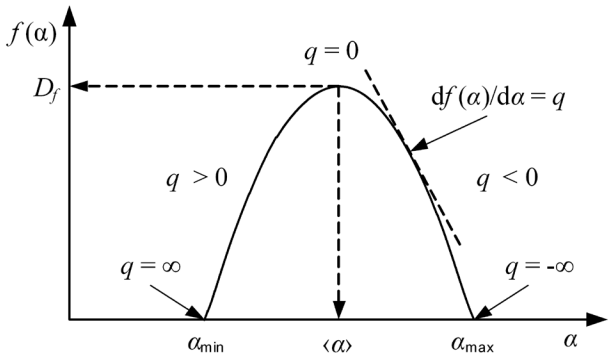

WAVELET TRANSFORM MODULUS MAXIMA METHOD

The method of Wavelet Transform Modulus Maxima (WTMM) was been proposed for the estimation of multifractal spectrum parameters by Hwang and Mallat (1994). The WTMM method has a number of essential advantages: a capacity for the analysis of a wide class of singularities-not only signals, but also their derivatives-the smaller inaccuracy of scaling characteristics evaluation, and so forth. WTMM technique, which can be successfully applied in examination of non-homogeneous structure of processes of a various nature, is based on the wavelet analysis named mathematically "microscope" in view of its ability to save good resolution on different scales.

Attractiveness of the given method consists in its possibility to analyze both singular measures, and singular functions. The method is a more general-purpose means of examining the multi-scaling properties of objects in comparison with earlier developed approaches.

In spite of the fact that in WTMM at the intermediate stages the wavelet-transform is used, it represents a combination of two different theories namely – the wavelet theory and the theory of multifractals. For the analysis of the input signal $s(t)$ we execute n continuous wavelet-transforms $(n = log_2 N,$ where N – is length of the signal) with the mother wavelet $\psi(t)$ on a scale level (or octave) of j:

$$W_s(u, j) = (s(t), \psi_{u,j}(t)) = 2^{-j/2} \int_{-\infty}^{\infty} s(t)\psi\left(\frac{t-u}{2^j}\right)dt, \quad (24)$$

As shown by Mallat (2005), if function $s(t)$ is self-similar then its wavelet-transform $W_s(u, j)$ also has the property of self-similarity. The concept of self-similarity in wavelet-transform presupposes that the positions and magnitudes of its modulus-maxima are also self-similar.

S. Mallat in (Mallat, 2005) proved that the singularity of non-stationary signals (e.g. multifractal signals) can be detected using WTMM global partition function. By employing WTMM in the computation of the global partition function, deviations engendered by the oscillation of wavelet-coefficients when $q < 0$ may be avoided. WTMM is a more accurate and correct approach to detecting the singularity of a signal. Hence, it is possible to measure the spectrum of the peculiarities of a multifractal signal from local maxima of the wavelet-transform, using the global partition function introduced by Muzy et al. in (Muzy, Bacry, & Arneodo, 1994).

Let ψ be a wavelet with n zero moments. It is proven that if s has smooth *Lipschitz* points $\alpha_0 < n$ at point ν, then wavelet-transform $W_s(u,j)$ has a

reference $\tau(q) = (q-1)D_q$ on $q\frac{d\tau}{dq} = D_q + (q-1)D'_q = \alpha(q)$ and supposing that $q = 1$, we find that $\alpha(1) = D_1$. Thus, $D_1 = \alpha(1) = f(\alpha(1))$. i.e. the informational dimension D_1 lies on the curve $f(\alpha)$ at the point, where $\alpha = f(\alpha)$ and $f'(\alpha(1)) = 1$. This gives us a graphic way to determine the informational dimension on the curve $f(\alpha)$ (see Figure 2). Now let's consider the case when $q = 2$. We have $D_2 = 2\alpha(2) = f(\alpha(2))$ or $f(\alpha(2)) = 2\alpha(2) - D_2$, which corresponds with the geometric construction on the Figure 3.

The multifractal dimension of the q^{th} order is determined by Equation (23)

$$D_q = \frac{1}{q-1}\left[q\left(\alpha(q) - f(\alpha(q))\right)\right] \qquad (23)$$

Using numerical methods of estimating the scaling function we can find an analytic expression for the spectrum of singularities. For example, if the scaling function is described by the formula

$$\tau(q) = -a_0 + a_1 q - a_2\frac{q^2}{2!} + a_3\frac{q^3}{3!} = \sum_{i=0}^{3} a_i q^i,$$

then in the quadratic approximation the spectrum of singularities (Figure 4) is as follows: $f(\alpha) = a_0 - \frac{(\alpha - a_1)^2}{2a_2}$, where the boundaries of the interval satisfy the equation :

$$\alpha_{\min,\max} = a_1 \pm \sqrt{2a_2 a_0}, \text{ or } q^*_{\pm} = \pm\sqrt{2a_0/a_2}.$$

This situation is qualitatively reflected in Figure 4. Also shown are the boundaries of the interval $(\alpha_{min}, \alpha_{max})$, in which the function $f(\alpha)$

Figure 2. Finding the information dimension $D_1 = \alpha(1) = f(\alpha(1))$

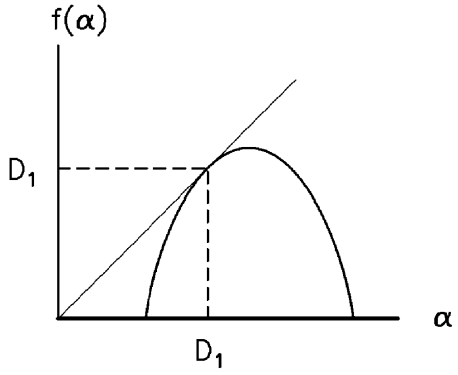

Figure 3. Geometric definition of the correlation dimension D_2

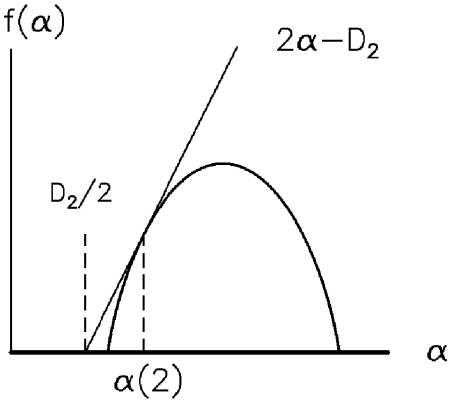

is set. It is necessary to specify that the conversion of the function $f(\alpha)$ to zero in this range (as shown in the figure) does not always occur and in some other cases $f(\alpha)$ in one of these points (or in both) may differ from zero. A prerequisite, however, is the conversion of the derivative $f'(\alpha)$ to infinity at these two points.

$p_i \approx 1 / N(\varepsilon)$). As a result, we have the following important inequality for the function $f(\alpha)$. For all possible values of α

$$f(\alpha) \leq \alpha \tag{17}$$

With equality *iff* the fractal is completely homogeneous in which case $f(\alpha) = \alpha = D$.

Researches reported in the literature have shown that the multifractal spectre of real data $f_G(\alpha)$ is difficult to calculate directly (Sheluhin, Smolskiy, & Osin, 2007). It can however be easily calculated by means of the Legendre transformation, giving the Legendre's spectrum $f_L(\alpha)$. $f_L(\alpha)$ is the same as $f_G(\alpha)$ provided that $\tau(q)$ exists and is differentiable for all valid values of q. The following expressions define the Legendre transformation from variables $\{q, \tau(q)\} to \{\alpha, f(\alpha)\}$:

$$\tau(q) = q^{2}\alpha(q) - f(\alpha(q)) \tag{18}$$

$$\alpha = \frac{d\tau}{dq} \tag{19}$$

$$f(\alpha) = q\frac{d\tau}{dq} - \tau \tag{20}$$

where $\tau(q)$ is the scaling index or the scaling function.

The inverse Legendre transformation is defined by the following formulas:

$$q = \frac{df}{d\alpha} \tag{21}$$

$$\tau(q) = \alpha\frac{df}{d\alpha} - f \tag{22}$$

For a homogeneous fractal $D_q = D = const.$ Which is the reason why $\alpha = d\tau / dq = D$, and $f(\alpha) = q\alpha - \tau(q) = qD - D(q-1) = D$. In this case, plot of the function $f(\alpha)$ on the plane $\{\alpha, f(\alpha)\}$ consists of one point only (i.e. $\{D, D\}$).

The authors consider more interesting cases when the graph of the function $f(\alpha)$ consists not of discrete points, but represents a continuous line. Since $f'(\alpha) = q$, then for $q = 0$ the derivative of the function turns to zero. This means that at some point $\alpha_0 = \alpha(0)$ the function $f(\alpha)$ has a maximum (keeping in mind that the function $f(\alpha)$ is convex). The function's value at the maximum $f(\alpha_0) = D_0$, i.e. the maximum value of $f(\alpha)$, is equal to the Hausdorff dimension of the multifractal D_0 (see Figure 1).

Now consider the case when $q = 1$. As $\tau(1) = 0$, then $\alpha(1) = f(\alpha(1))$. On the other hand, the derivative of the function $f(\alpha)$ at this point equals 1: $f'(\alpha(1)) = 1$. Differentiating the

Figure 1. Function maximum is equal to the fractal dimension of D0

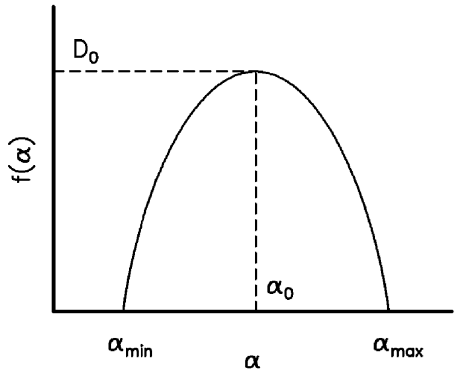

Service (DoS) and different types of unauthorized network sniffing. DoS attacks also incorporate Distributed DoS attacks (DDoS) which entail the enslavement of a number of host computers for the purposes of unleashing attack on a single victim. Various anomalous network *sniffings* are indicative of hacker events as well as acts of harmful programs (worms). Suffice it to note here that network traffic with different types of attack differed significantly in comparison with the normal scenario. This difference affected the throughput at both the packet and bit level as well as the connection usage and consequently the volume of transmitted data. The change in network traffic characteristic can be observed visually. But a visual observation alone cannot suffice, since the manner in which the changes occur and their representations in the form of mathematical models are problems that must be studied with the instrumentation of mathematical tools.

In considering the features of WTMM method used for the detection of anomalies in the traffic with DoS attacks, $n = \log_2 72,700 = 16$ continuous wavelet-transforms of the input realization was performed. The spectrograms for selected octaves are shown in Figure 6 (Sheluhin, Atayero, & Garmashev, 2011).

The spectrograms clearly reveal a frequency-time localization of all the features of the signal. For example, the abnormal spike in the region of $n = 6{\cdot}10^4$ s (Figure 6 a, b, c) manifests as abrupt disturbances in the spectrogram, this is evidently absent in the same region of Figure 5a.

It is appreciable at decomposition levels approximately from 1 to 11 (Figure 6a). As the mother wavelet scale becomes more than anomaly time period, it ceases to be fixed on the spectrogram. The mother wavelet scale at 16th level of decomposition (Figure 6c) is proportionate to all length of the implementation, therefore actually any time-and-frequency singularities is not watched. Therefore, spectrogram analysis suggests that some features of the signal can manifest themselves at some level of decomposition, but not at other levels, therefore to identify all the features of the signal it is analyzed on all octaves.

Figures 7a through 7d show the partition functions $S\left(q,j\right) = \sum_P \left|W_S\left(u_p,j\right)\right|^q$ for an octave j=16 are represented.

Partition functions for implementations with anomalies and without have considerable differences. Figure 7b and 7d, show that the statistical sum at $q < 0$ is characterized by the presence of specific peaks, at $q > 0$, the partition function is much more smooth. To analyze differences, we consider partition functions for the positive and negative values q separately (Figure 8a, 8b).

Figure 8a shows that though differences are available, they are insignificant and cannot serve as criteria for anomalous activity determination. It is possible to tell that partition functions at

Figure 5. Implementation of network traffic: a) network without anomaly and b) network with abnormal activity

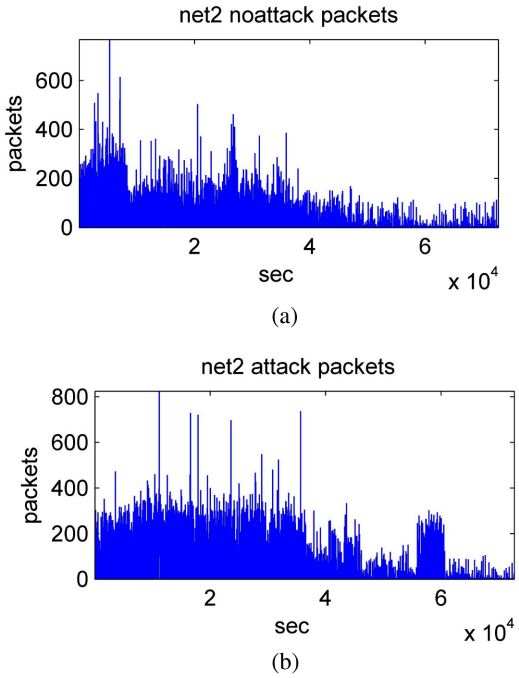

Figure 6. Spectrograms of wavelet-transform: at the left - for network without attacks, at the right – for network with anomalies and rejections a) octave j=11, b) j=13, c)j=15

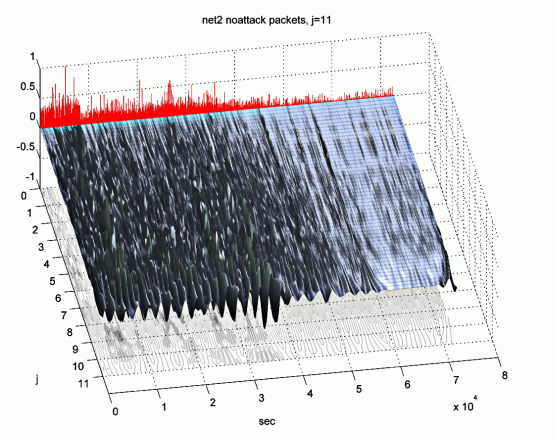

(a1)

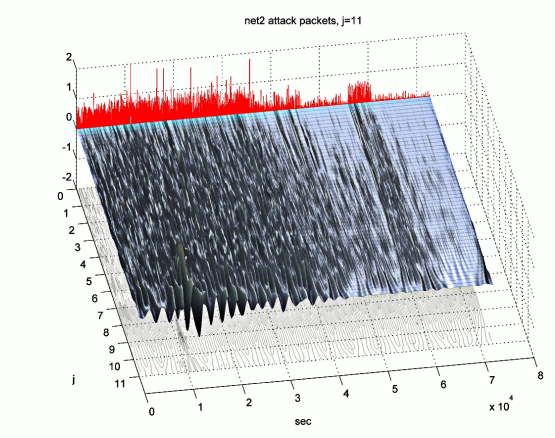

(a2)

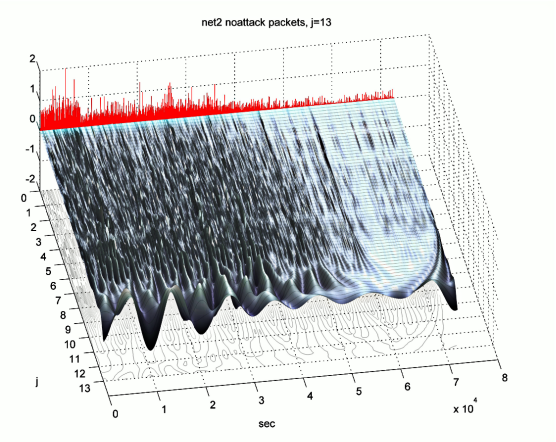

(b1)

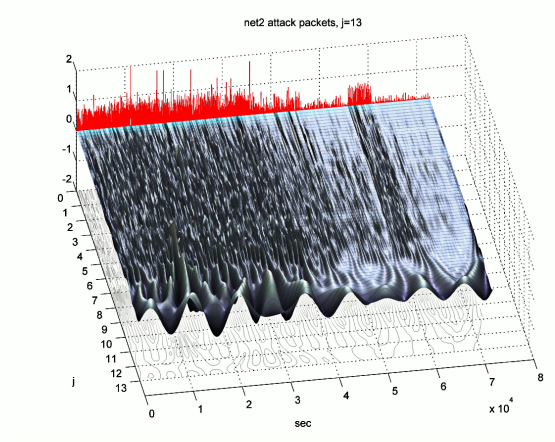

(b2)

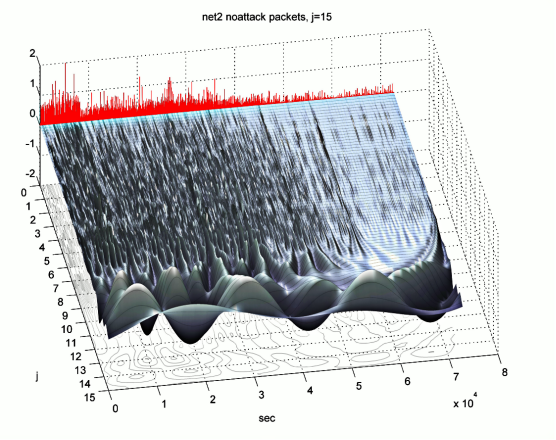

(c1)

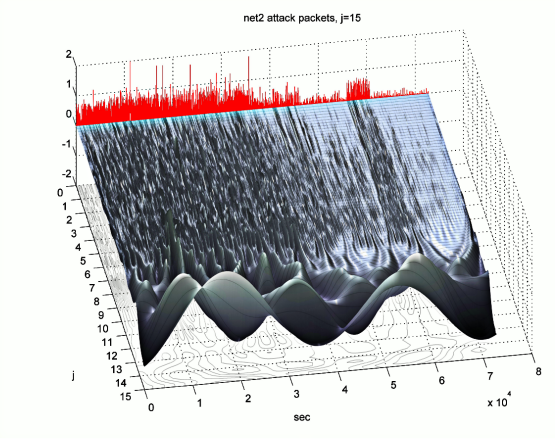

(c2)

$q > 0$ responsible more likely for similarity, than for differences of two implementations. It is necessary to remind that the left "wing" of the multifractal spectrum function $f(\alpha)$ corresponds to values $\alpha at q > 0$. Furthermore, it will be shown that similarity of some implementations is exhibited in this part of a singularities spectrum. Now we consider a partition function for values $q < 0$ (Figure 8b).

On this figure differences are accurately visible. They are characterized by distinction of values and position of peaks (maximas) of a partition function on an axis of scales. Thus, presence of peaks at a partition function at $q > 0$ at some decomposition scale level *j* speaks about presence on its high-frequency local maximas. Presence of peaks at $q < 0$ talks about the accumulations of low-amplitude local maximas, which in turn speaks about local singularities of a signal decomposition on the given octave. It is possible to make a conclusion that various values and positions of peaks on decomposition scale axis indicate various frequency characteristics of a signal on the same octave that speaks about their principle distinction.

Figure 7. Partition function for j=16: a, b) implementation without anomalies, c-d) with anomalies

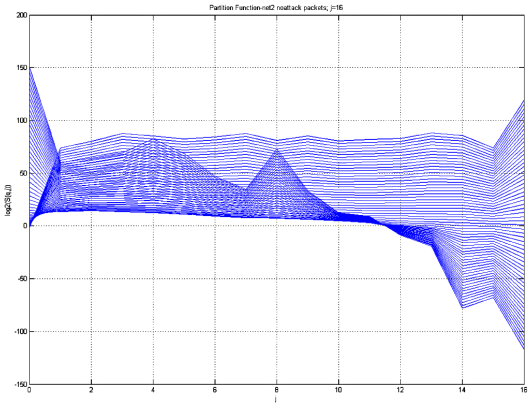

(a)

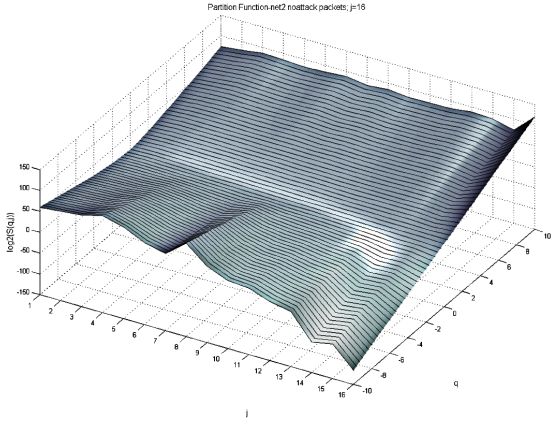

(b)

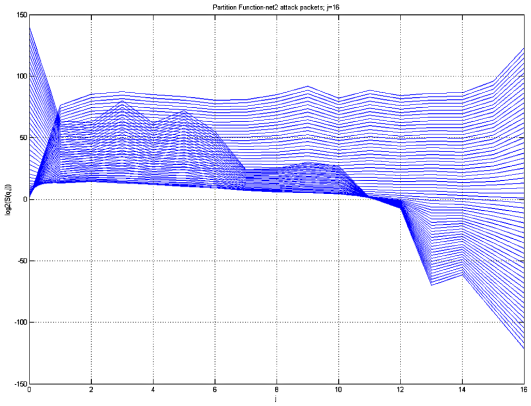

(c)

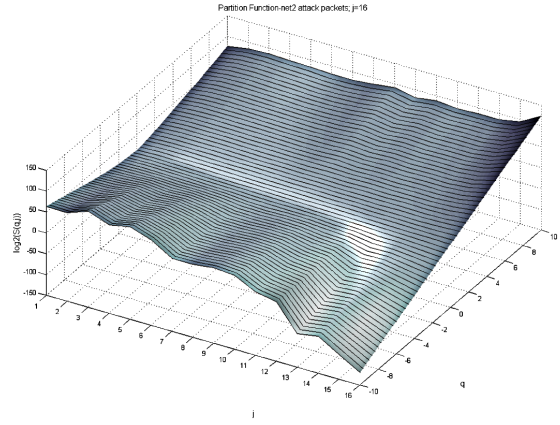

(d)

Figure 8. a) Partition functions at q> 0, j=16: on top implementation without anomalies, from below - with anomalies; b) partition functions at q <0, j=16: on top implementation without anomalies, from below - with anomalies

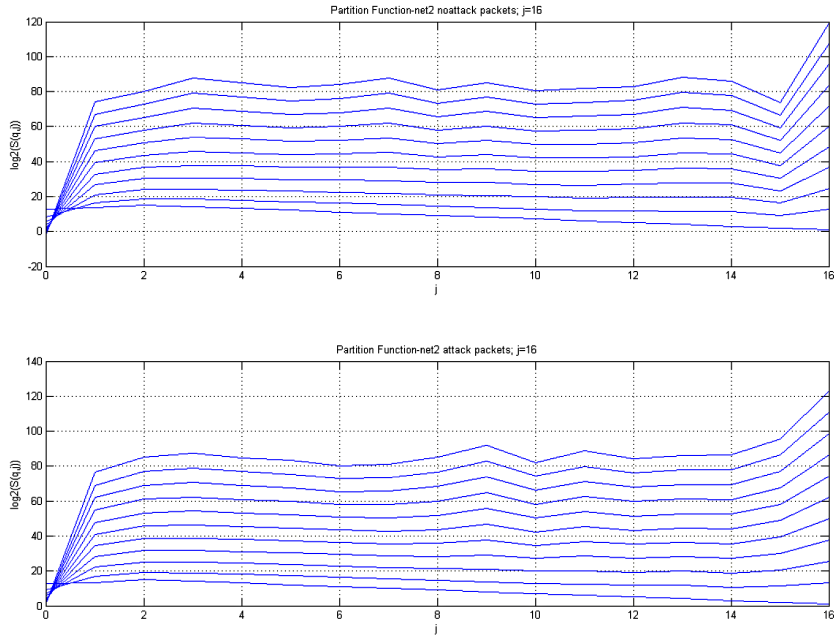

(a)

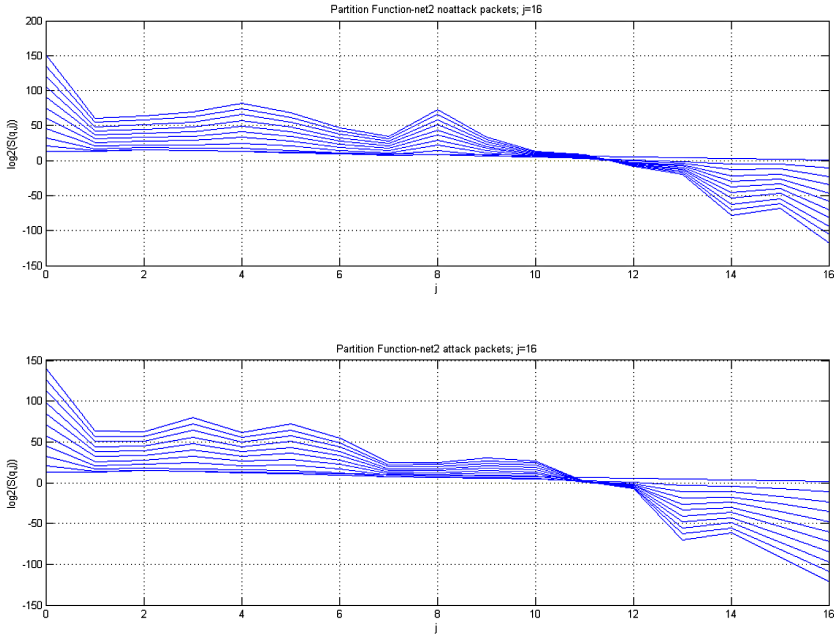

(b)

On Figure 9-a-d results of the scaling function $\tau\left(q,j\right)$ evaluation are shown.

Figures 9a through 9f show that also, as well as in case of a partition function, there are distinctions in $\tau\left(q,j\right)$, and are exhibited in slope of functions. Figure 9e and 9f of scaling functions illustrate the typical nonlinearity and convexity. The multifractal spectrum, which as it is shown in Figure 10, estimated from $\tau\left(q,j\right)$ by means of Legendre transform (28) characterizes essential differences of two implementations.

On Figure 10 results of singularity spectrum evaluations are shown.

Figures 10a through 10d clearly show that increasing scale decomposition levels involved in the analysis, computation of the spectral maximum (Hausdorff dimension) and its sampling interval, each previous spectrum seems embedded in the next, (i.e. the spectrum gets more accurate from one octave to the next). This suggests that the higher the level of decomposition, the more features the signal spectrum depicts. Figure 11 clearly illustrates that the spectra of realizations with and without anomalies are different for each scaling decomposition level j. From octave to octave spectra of normal and attacked network have practically the same Hausdorff dimension, due to the fact that the analyzed the realizations are of equal length. However, other dimensions are significantly different. Particularly large differences are manifested towards the right wing of the spectrum for $q < 0$. It is seen that due to the fact that the sequences have the same length, Hausdorff dimension of the multifractal $f\left(\alpha_0\right) = D_0$ remains virtually constant (maxima of the functions are the same). But its information dimension D_1 and correlation dimension D_2 differ. The boundaries α_{min},α_{max} in which the function $f\left(\alpha\right)$ is given also differs. Thus, the differences in the characteristics of traffic with and without anomalies are clearly reflected in the plots of their singularity spectra, which can be found using the WTMM method. Formalizing how spectra differ from each other, these dimensions can be compared as well as the function generation intervals. We find the Hausdorff dimension D_0, the information dimension D_1, correlation dimension D_2 and the intervals that characterize the "width" of the Legendre spectrum for each of the realizations on each decomposition octave. A comparison of these parameters is summarized in Table 1.

Based on the obtained parametric values, a plot of the multifractal dimensions *D* as a function of octave *j*, can be drawn for comparing the two realizations (Figure 12). Analysis of the presented relationships shows that the differences between two realizations are manifested in their multifractal spectra, constructed using the developed software based on WTMM method, regardless of the amount of levels of scaling decomposition (octave) *j* involved in the analysis. The characteristics of the spectrum at each level of decomposition can reveal the local features of the signal, allowing for their detection by means of analyzing the multifractal spectra of realizations for a given level of decomposition.

Hausdorff dimension of the realization under comparison D_0, which determines the number of local maxima found for a given number of decomposition levels differs most for small values of decomposition (octave) levels. Information dimension of realizations being compared D_1, responsible for the difference in the left slopes of the multifractal spectrum differ by a small but constant value and is practically independent of the number of levels of decomposition.

We safely conclude that the presence of diverse and continuous attacks and anomalous activity in a signal changes the self-similar nature of traffic a fact indicated by the difference in the information dimensions D_1. Correlation dimension D_2 varies smoothly from octave to octave, displaying similar values at levels 9-11. It may be said that D_1 characterizes local features of the signals over

Table 1. Characteristics of the multifractal spectrum: (Realizations without anomalies (N) and those with anomalies (A))

Par.	$j=7$		$j=8$		$j=9$		$j=10$		$j=11$		$j=12$		$j=13$		$j=14$		$j=15$		$j=16$	
	N	*A*	*N*	*A*	*N*	*A*	*N*	*A*	*N*	*A*	*N*	*A*	*N*	*A*	*N*	*A*	*N*	*A*	*N*	*A*
D_0	0.370	0.458	0.513	0.577	0.630	0.666	0.723	0.727	0.773	0.771	0.807	0.806	0.835	0.833	0.856	0.854	0.872	0.874	0.893	0.892
D_1	0.342	0.419	0.497	0.553	0.615	0.655	0.715	0.727	0.773	0.771	0.807	0.797	0.823	0.810	0.836	0.821	0.844	0.834	0.859	0.846
D_2	0.959	0.876	0.641	0.576	0.430	0.420	0.348	0.343	0.332	0.344	0.308	0.368	0.383	0.488	0.495	0.564	0.587	0.673	0.682	0.780
α_{min}	0.572	0.478	0.458	0.364	0.352	0.330	0.268	0.290	0.206	0.242	0.158	0.210	0.146	0.184	0.146	0.158	0.136	0.162	0.150	0.184
α_{max}	0.712	0.768	0.654	0.706	0.648	0.680	0.714	0.698	0.766	0.764	0.794	0.822	0.884	0.944	0.988	1.028	1.076	1.122	1.156	1.204

time moment -*t* in the past until a moment in present *t=0*. The so-called workload process $Q(t)$ is the total amount storable in buffer at the interval $(-t\ ;0)$.

Let's define current length of the queue buffer as $Q(t,r)$ which is the queue length in an equilibrium state when the system has been running for a long time and initial queue length has no influence. If such state of system exists (i.e. the supposition of stationarity and ergodicity of workload process is valid) and the state of system stability also satisfied, then

$$Q\left(t;r\right)=\sup_{0\le S\le t}\left(A\left(t\right)-A\left(s\right)-r\left(t-s\right)\right) \quad (32)$$

Here $\left(A\left(t\right)-A\left(s\right)\right)-$ is the value of workload, received for processing during time interval $\left[s,t\right]$; $r(t-s)-$ is the value of workload processed in the same time interval.

Input process $A\left(t\right)$ is considered a fractal process of the type given in (33)

$$A\left(t\right)=\lambda\ ^{2}t+\sqrt{a\ ^{2}\lambda\ ^{2}Z\left(t\right)}\ \ ;\ t\in\left(-\infty\ ;+\infty\right) \quad (33)$$

where $Z(t)-$ is the normalized fractal Brownian motion,

$H\in\left[1/2;1\right)-$ is Hurst parameter of process $Z\left(t\right)$;

$\lambda>0-$ is average input intensity;

$a>0-$ is modification coefficient and

$r>\lambda-$ is service rate.

Equations system (32) and (33) are completely characterized by four parameters: $\lambda\ ,a\ ,H\ and\ r$. The self-similarity of process $Z\left(t\right)$ allows for obtaining more exact ratios between network parameters - buffer length *L*, channel transmission capacity *C* and traffic parameters *r, a* and *H* for boundary values from Equation (33).

The analysis of queuing performance with *fBm* input traffic was presented for the first time by Norros (1994), where it was shown that the distribution of queue length can be approximated by Weibull distribution. In was particularly reported by Norros (1994) that the queue tail distribution in the case of a *fBm* input satisfies the equation:

$$\log\left(P\left[Q>L\right]\right)\approx-\frac{1}{2}L^{2\left(1-H\right)}r^{2H}\left(1-H\right)^{-2\left(1-H\right)}H^{-2H} \quad (34)$$

for sufficiently large values of *L*.

oriented on uncorrelated request flows in the conditions of the self-similar traffic yield excessively optimistic results. After detection of fractal structure in the network traffic the analysis of queuing performance for the fractal traffic on an input within the limits of the classical theory of queues become problematic. The results of some important researches (Brichet, Roberts, Simonian, & Veitch, 1996; Giordano, O'Connell, Pagano, & Procissi, 1999; Lui, Nain, Towsley & Zhang, 1999; Norros, 1994) are published in the literature. The influence of fractality on research on creation of queues is an important problem. Some applications of network design, such as setting buffer size and traffic management are connected to this problem, which makes it extremely important.

MODEL OF QUEUING WITH TRAFFIC DESCRIBED BY FRACTAL BROWNIAN MOTION (FBM)

Let's consider a simple model of queuing: queue of the separate server. It is considered in the continuous time, the serving principle is set to FIFO. We assume that queue has the infinite buffer and constant service rate r. Denote as $A(t)$ a total amount of workload arriving to the queue from a

Figure 12. Multifractal dimensions comparison of two realizations (circle– D0 , dots–D1, triangle–D2): blue–dimensions for network without attack; red–dimensions for network with attack

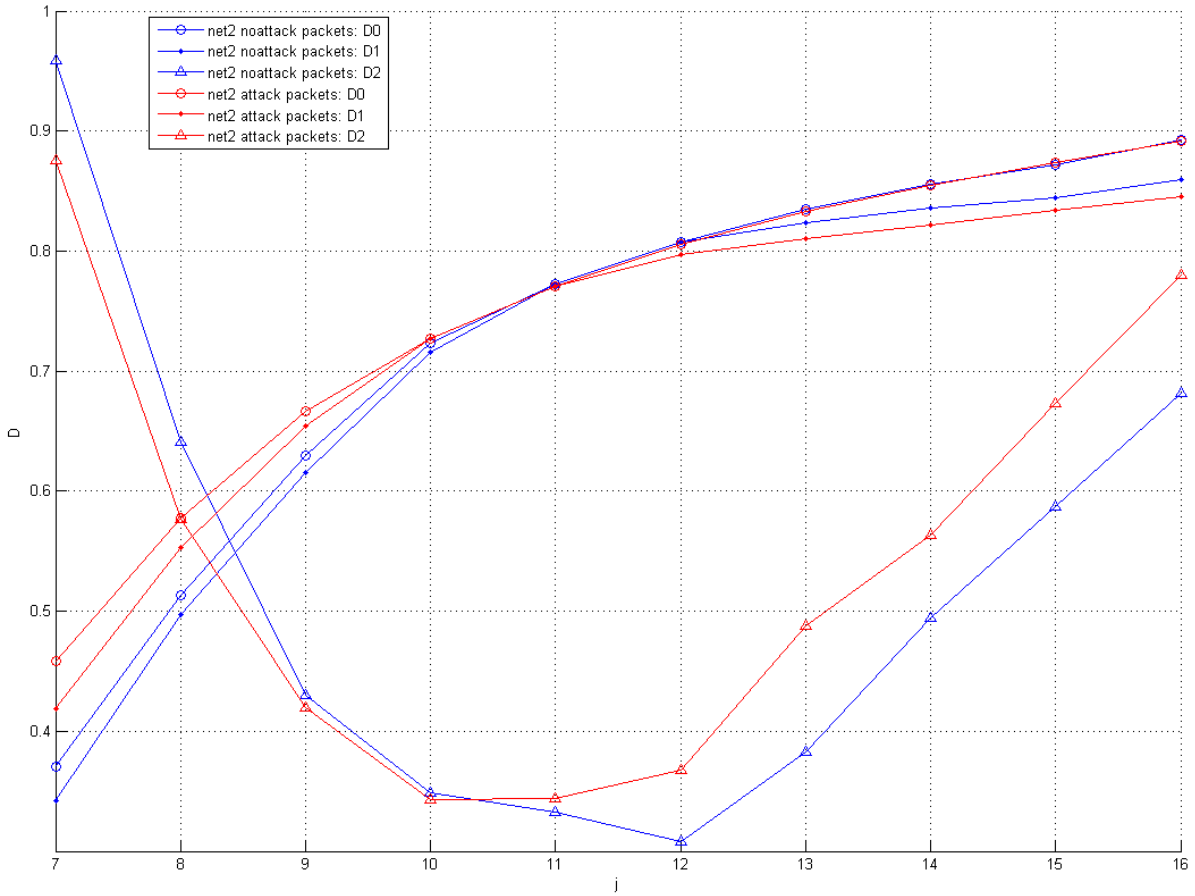

Figure 11. Multifractal spectra in comparing, black - without anomalies, white - with anomalies

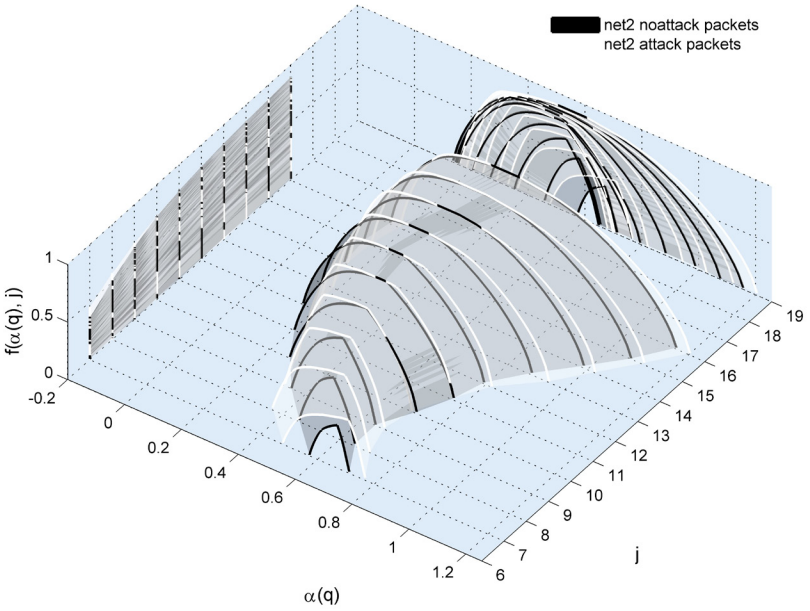

buffer capacity. For the Markov traffic processed in such queue, distribution of tails is approximately exponential (Park & Willinger, 1999).

$$P\left\{Q > B\right\} \sim e^{-\eta B} \ , as\, B \to \infty \qquad (30)$$

where $\eta > 0-$ asymptotic decay rate.

Expression (30) is taken as a principle concept of effective transmission capacity, where access control or the arranged capacity of the service channel is based on a tails probability distribution of a random variables choice. Unlike (30) traffic flows with long-range dependence (in particular, the models based on fractal Brownian motion) lead to tail queue distribution that decays asymptotically with a Weibullian law, that is

$$P\left\{Q > B\right\} \sim e^{-\gamma B^{\beta}} \ , as\, B \to \infty \qquad (31)$$

where $\gamma -$ is a constant, and $\beta = 2 - 2H \in (0\ ;1]$.

Formulas 30 and 31 strongly differ. The first on comparing with the second gives rather optimistic predictions. The question about, whether other traffic models lead to correct, in comparison with experimental data, prognoses of network productivity, till now remains open. The general analytical results of queuing performance, or influences of traffic self-similarity and long-range dependence on Quality of Service (*QoS*) do not exist at present. Only separate analytical results for special cases are known. At the same time the most effective method of an overall performance estimation of telecommunication networks remains, obviously, simulation-modeling methods. From these positions problems of influence of a traffic self-similarity level on telecommunication systems efficiency will be considered in the following section.

THE MONOFRACTAL TRAFFIC

When designing any telecommunication network one has is faced with restrictions on transmission capacity of channels. In these conditions the estimation of effective band pass range becomes one of the key problems. Calculations on the basis of classical methods of queuing theorems

Figure 10. Dependence of a multifractal spectrum on an amount of scale levels involved in the analysis j, j=0…16. a, b) for a network without anomalies, c, d) - for a network with anomalies

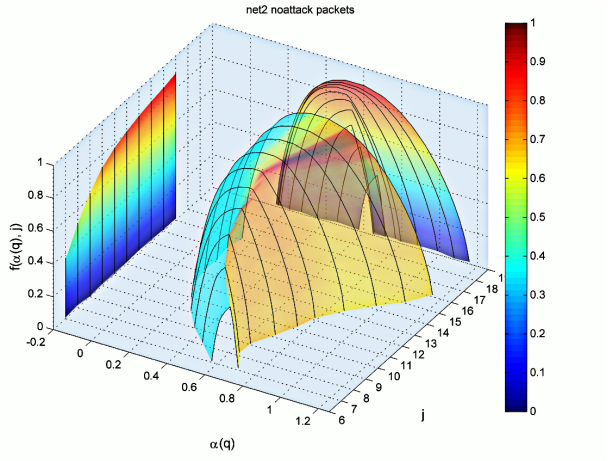

(a)

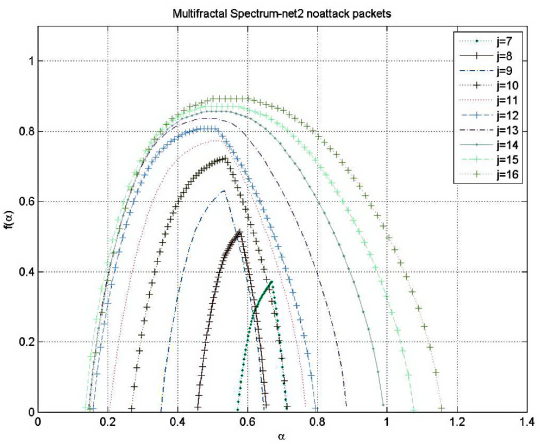

(b)

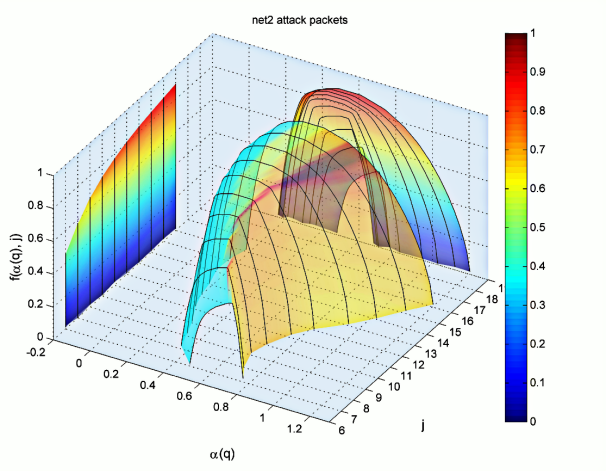

(c)

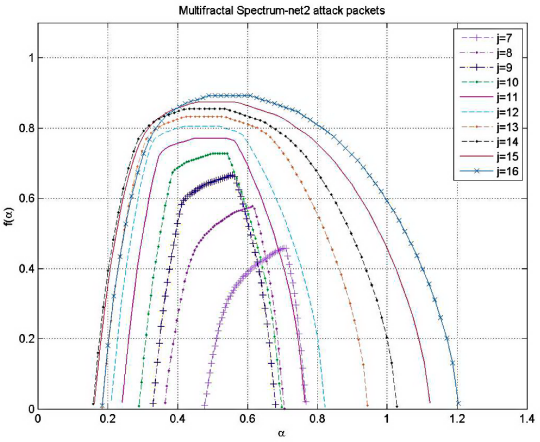

(d)

the levels of decomposition and can thus be used to detect anomaly at a given level of decomposition.

The values of boundary parameters of the spectra α_{min} and α_{max} almost always show different values for two realizations and can likewise serve as a reliable distinguishing characteristic of multifractal spectra and indicator of the presence of abnormal activity.

ESTIMATION OF THE IMPACT OF TRAFFIC MULTIFRACTALITY ON QUEUING PERFORMANCE IN TELECOMMUNICATION NETWORKS

Results of numerous researches show that measurements of queuing performance of a fractal traffic can essentially differ that are predicted by appropriate systems with traditional traffic patterns. It is interesting in this context the distribution tails behavior of queue of length Q in a stable condition for one server with infinite queue

Figure 9. Functions τ(q, j): for scale levels j=0 …16 a-d) at the left - for a network without attacks, on the right - for a network with anomalies; e)-for an octave 13 in comparing; f)-for an octave 15 in comparing

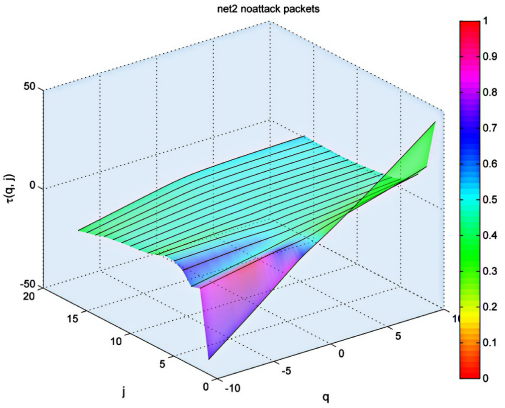

(a)

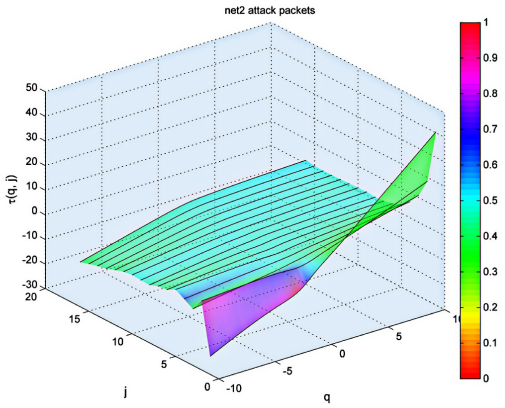

(b)

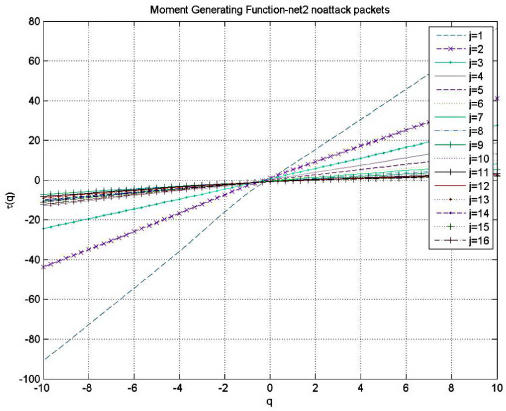

(c)

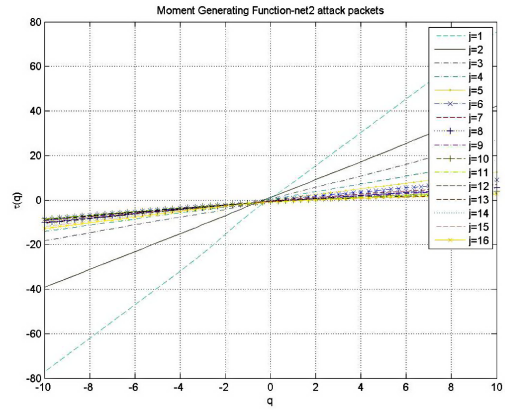

(d)

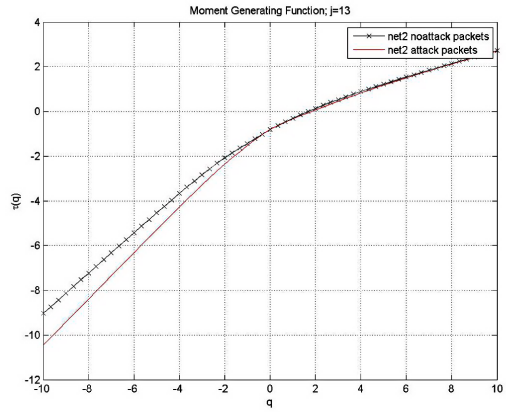

(e)

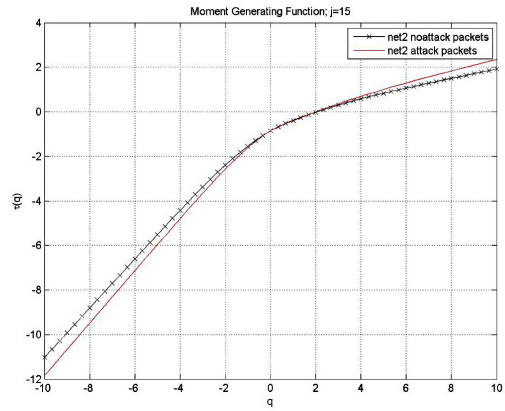

(f)

to the right by k scale units from origin of the coordinate system; $D_j\left(t\right)=\sum_{k=0}^{n_0/2^j-1} d_{j,k}\ ^2\psi_{j,k}\left(t\right)-$ j-scale order detailed function; $d_{j,k}=<X\left(t\right),\psi_{j,k}>-$ wavelet coefficient of scale j, equals scalar product of initial series $X(t)$ and wavelet of scale j, shifted to the right by k scale units from origin of the coordinate system.

The resultant discrete wavelet transform presents a series X of size n on scale j, derived by the means of wavelet coefficients set $d_X(j,k),k=1,2,\ldots,n_j$, where $n_j=2^{-jn}$ and $n-$ accessible number of wavelet coefficients in octave j.

Phase 2: Definition of q^{th} logarithmic order diagram of the q^{th} moment of octave j:

$$\mu\left(j,q\right)=1/n_j\sum_{k=1}^{n_j}\left|d_X\left(j,k\right)\right|^q \qquad (37)$$

The sum in expression (37) is taken of points in space, where the wavelet transform modulus can take maximum values (i.e. on local maxima

Figure 17. Results of multifractal analysis of sampled data: a) decomposition function $\mu\left(j,q\right)$; b) function $\tau\left(q\right)$; c) dependence $\log_2 c\left(q\right)$; d) multifractal spectra $f(\alpha)$ at $q>0$

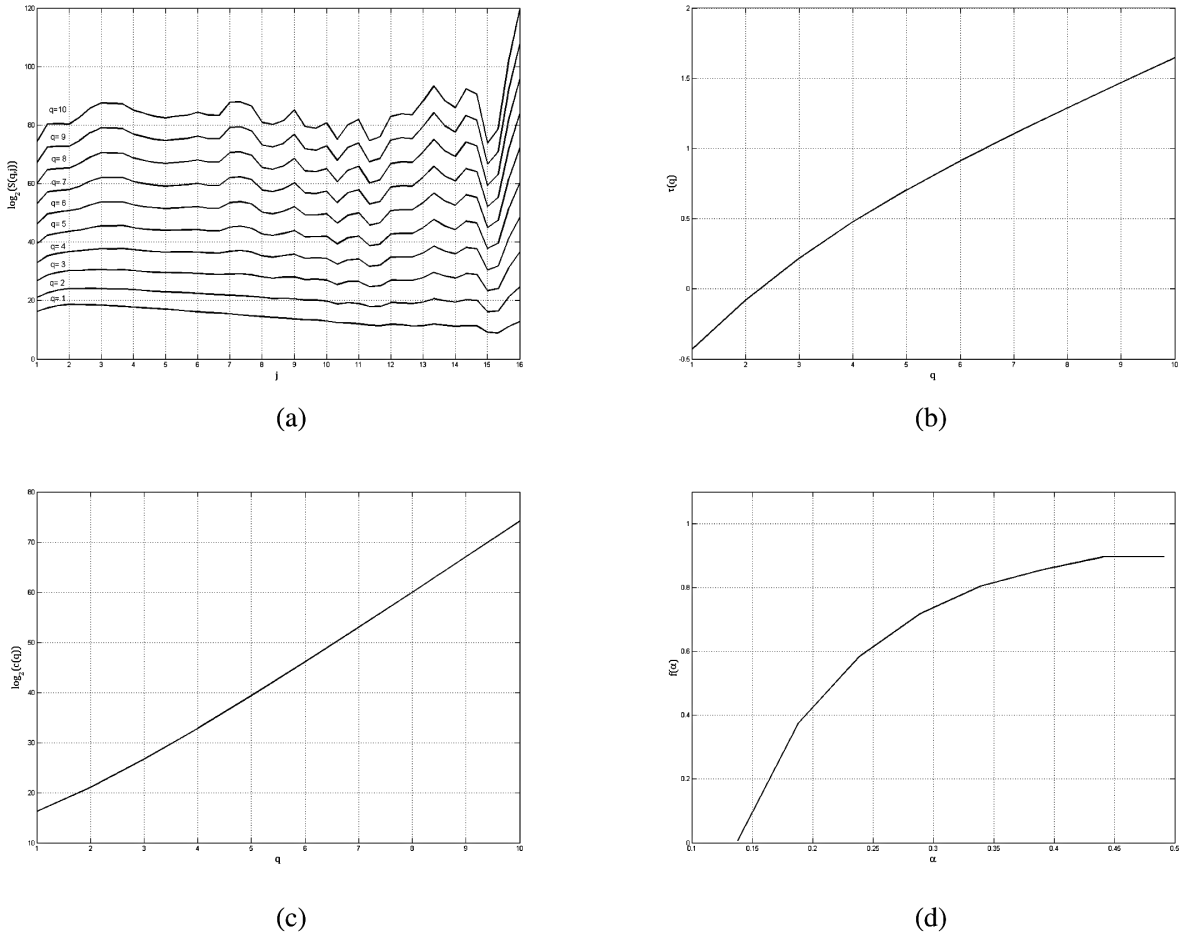

(a) (b)

(c) (d)

Table 2. Approximation coefficients

Function $\tau(q)$				**Function** $\log_2 c(q)$			
a_0	a_1	a_2	a_3	c_0	c_1	c_2	c_3
-0.8260	0.4249	-0.0296	0.0012	11.8325	3.9479	0.3873	-0.0160

wavelet analysis, we represent the time series $X(t)$ as follows:

$$X(t) = X_J(t) + \sum_{j=1}^{J} D_j(t)$$

where $X_J(t) = \sum_{k=0}^{n_0/2^J-1} S_{J,k} \cdot \varphi_{J,k}(t)$ – initial approximation function, conforms to scale J ($J \le J_{\max}$);

$S_{J,k} = < X(t), \varphi_{j,k} >$ – scale coefficient, equals to scalar product of initial series $X(t)$ and scaling function with "*roughest*" scale J, shifted

Figure 16. Traffic data for analysis

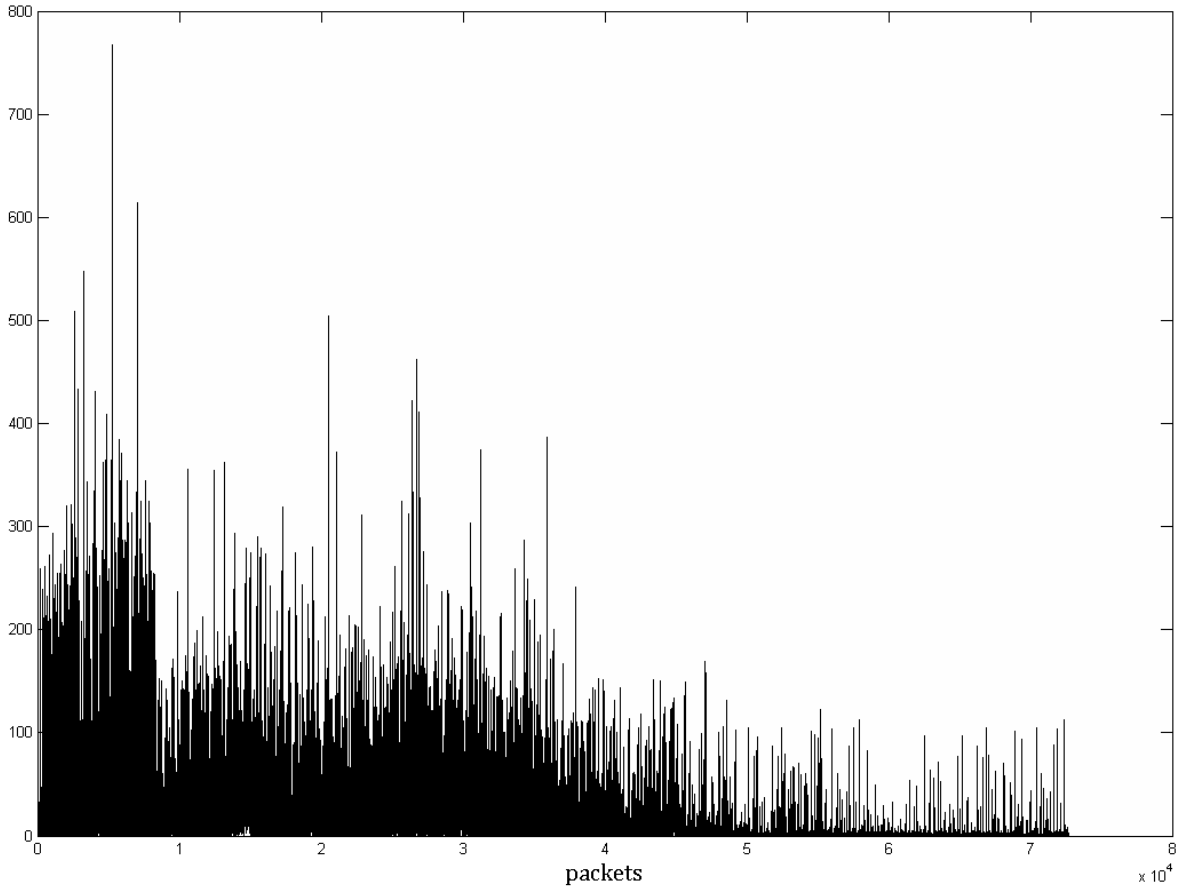

only determined form of scaling function $\tau_0(q)$ and moment coefficient $c(q)$ could provide a final result. The reason for this consists in the definition of multifractal process class, that doesn't impose any restrictions on functions $c(q)$ and $\tau_0(q)$ (except that $\tau_0(q)$ is a convex function). Investigation of queuing performance systems with summarized multifractal traffic shows that it can provide some similarity with monofractal inbound process generalized results. Equation (36) shows that the queue distribution characteristic in case of multifractal traffic input is completely characterized by the scaling function $\tau_0(q)$ and scale coefficient $c(q)$ of the input traffic.

ESTIMATION METHODOLOGY FOR FUNCTIONS $c(q)$ AND $\tau_0(q)$ IN THE CASE OF ARBITRARY MULTIFRACTAL INBOUND PROCESS

Phase 1: High definition measurement of inbound entry process $X(t)$. Assume that inbound process shows multifractal scaling properties. Then scaling function $\tau(q)$ and function $c(q)$ can be estimated on the basis of recorded data for a number of possible parameters $q > 0$. It is important to note the role of function $c(q)$ as the quantitative coefficient of multifractal process, whose import is sometimes underestimated in researches on the evaluation of the multifractal properties of high-speed network traffic. Scaling function $\tau(q)$ determines the *multiscaling* quality of traffic only and does not suffice for multifractal model description neither does it suffice for the analysis of queuing performance models with multifractal inbound processes. Scaling behavior can be examined by means of wavelet representation methods.

Advantages of wavelet analysis follow from the fact that function of the basal wavelet itself shows a scaling property and consequently composes an optimal *coordinate system*, where it is possible to observe the scaling phenomenon. It likewise provides a stable scale behavior, detection and accurate measurement of parameters that describe this scaling behavior.

We execute the wavelet decomposition of a sequential sample given by

$$X(t):\left\{x(t_0),x(t_1),\ldots,x(t_{N-1})\right\}$$

of size $n_0 = 2^{Jmax}$,$(n_0 \le N)$, to a scale varying detail function. Here $J_{max} = \log_2 N -$ maximal number of decomposition scales, $\log_2 N -$ integer part of $\log_2 N$.

Scale index value $j = 0$ conforms to a maximum resolution case i.e. the most exact approximation achievable. It equals the original series $X(t)$ consisting of n_0 samples. Conversion to coarser resolution occurs with increase in $j(0 < j \le J_{max})$. In accordance with the rules of

Figure 15. Estimation of functions τ(q) and c(q)

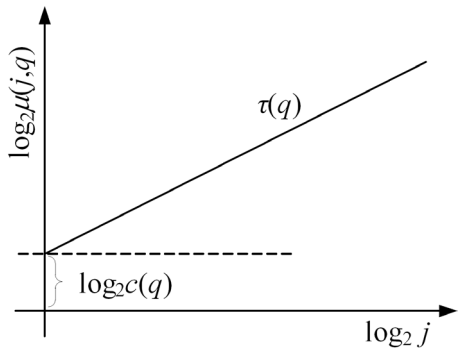

a and *H*. It is visible however, that when the buffer is small, requirements of the channel depend less on *H* than when the buffer is large. The observable outcome illustrates a well-established fact, that for short-range dependent traffic it is very difficult to fill big buffer sizes.

The obtained results show that queue distribution with *fBm* on an input has much smaller decay than in an exponential case. However, this approach is based on the Gaussian property of input process and cannot be spread to other processes with scale properties. There are only some analytical results for queuing performance for cases when the traffic has more complicated scale behavior. For example, there is a result when the input traffic is asymptotically self-similar and is described by the Pareto distribution, and for the case when Levi's distribution is used to describe the traffic.

TRAFFIC MULTIFRACTAL INFLUENCE ESTIMATION ON QUEUING PERFORMANCE

Queuing performance formulas in cases of Gaussian inbound processes lead to results that conform to the theory. For the generalized multifractal traffic a new practical method is proposed for queuing performance estimation.

APPROXIMATION OF QUEUE'S TAIL PROBABILITY

Researchers in (Dang, 2002) showed that probabilities of queue tail distribution asymptotes for queue construction model with single server and generalized multifractal inbound process are approximated correctly with Equation 36 (see Box 1).

As previously noted, scaling functions $\tau(q)$ and $c(q)$ are functions, which determine the multifractal inbound process. Considering Equation (36) it is evident it has an exact form, and

Figure 14. Transmission capacity of the channel as function of a at r = 2 Mbit\s and fixed; a) for L = 100Kbytes, b) for L = 1 MB

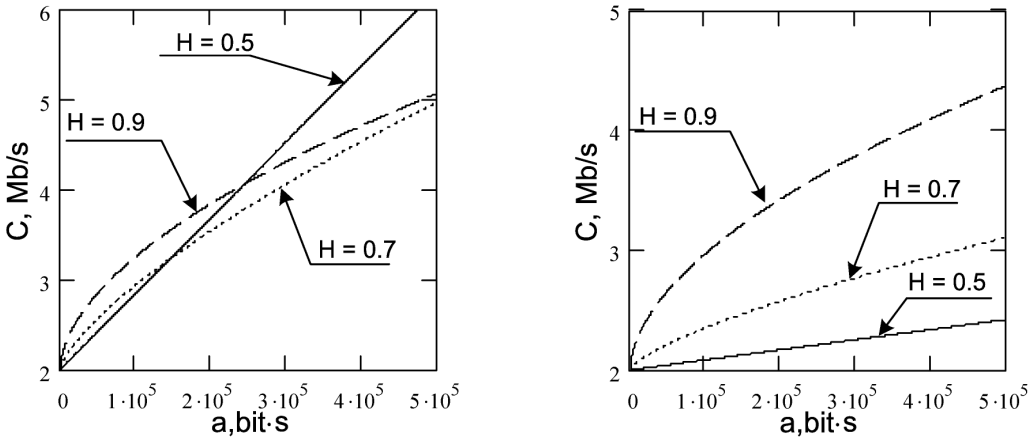

On Figure 13 dependencies of a queue tail approximation on a queue size L in log-log scale are presented at fixed *H* and *r*.

$$\log\left(P\left[Q > L\right]\right) = f\left(L\right) = -\log\left[\frac{1}{2} \cdot L^{2(1-H)} r^{2H} \left(1-H\right)^{-2(1-H)} H^{-2H}\right]$$

Observable linearity of the graph illustrates probability decay under the Weibull law.

Supposing that the probability $P\left(Q > L\right) = \varepsilon$ and $\rho = r / C$ it is possible to solve (34) *wrt C* and to discover that QoS is roughly reached, when Equation (35) holds

$$C = r + \left\{k\left(H\right)\sqrt{-2 \cdot \ln \varepsilon}\right\}^{1/H} \cdot a^{1/2H} \cdot L^{-(1-H)/H} \cdot r^{1/2H} \quad (35)$$

where $k\left(H\right) = H^H \cdot \left(1-H\right)^{1-H}$

For practical applications of Equation (35) as the formula determining the size of a channel, considering its sensitivity to *a* and *H* becomes something of interest. On Figure 14 channels characteristics with various values of *a* and *H* at $r = 2Mb / s, \varepsilon = 10^{-3}$ and for two buffer sizes $L = 100KB and 1MB$. Certainly, the same reservation as well as in the previous figure should be done at strict independence of modification of

Box 1.

$$\log\left(P\left[Q > L\right]\right) \approx \min_{q>0} \log\left\{c\left(q\right) \cdot \frac{\left[\frac{L \cdot \tau_0\left(q\right)}{r\left(q-\tau_0\left(q\right)\right)}\right]^{\tau_0(q)}}{\left[\frac{L \cdot q}{q-\tau_0\left(q\right)}\right]^{q}}\right\} \quad (36)$$

for sufficiently large values of L, where $\tau_0\left(q\right) = \tau\left(q\right) + 1.$

Figure 13. Dependence of queue tail approximation on a queue size L at a) r = 1 and fixed H, b) r = 5 and fixed H

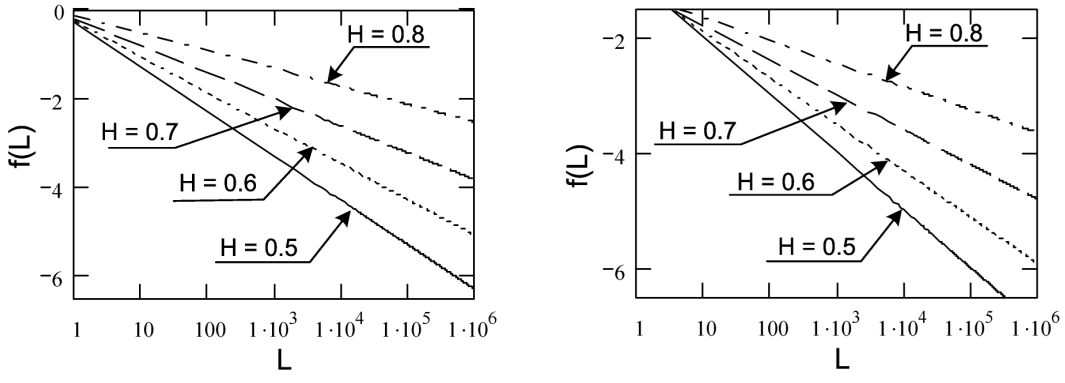

of modulus). Calculations of decomposition function (Renyi's function) allow for a trace of the scaling for large $(q > 0)$ and small $(q < 0)$ fluctuations.

We note once again that the sum of the second moments $\mu\left(j,q\right) = 2$ represents a variation of wavelet coefficients at their average value equal to zero. At $q > 0$ function $\mu\left(j,q\right) > 0$ describes a scaling of large fluctuations and strong singularities. At negative values of q, it is responsible for scaling of small fluctuations and weak features, thereby showing the sensitivity to different aspects of the dynamics underlying the investigated signal. Linearity of logarithmic diagrams at various orders of the moment q informs on the scaling property of the series, that is

$$\log_2 \mu\left(j,q\right) = \tau\left(q\right) \cdot \log_2 j + \log_2 c\left(q\right) \qquad (38)$$

where $\tau\left(q\right)$ is a scaling function, and $c(q) = const$.

The estimation method of $\tau(q)$ and $c(q)$ for the fixed value q is illustrated on Figure 15

This figure shows that the line slope characterises the scaling function $\tau(q)$, and the cut piece on the axis of ordinates is $\log_2 c\left(q\right)$. From Figure 15 and expression (38) we have that:

$$\tau\left(q\right) = \lim_{j\to\infty} \frac{\log_2 \mu\left(j,q\right)}{\log_2 j} \qquad (39)$$

Figure 18. Dependences lnP[Q>L] from lnL at r =2 and r = 5

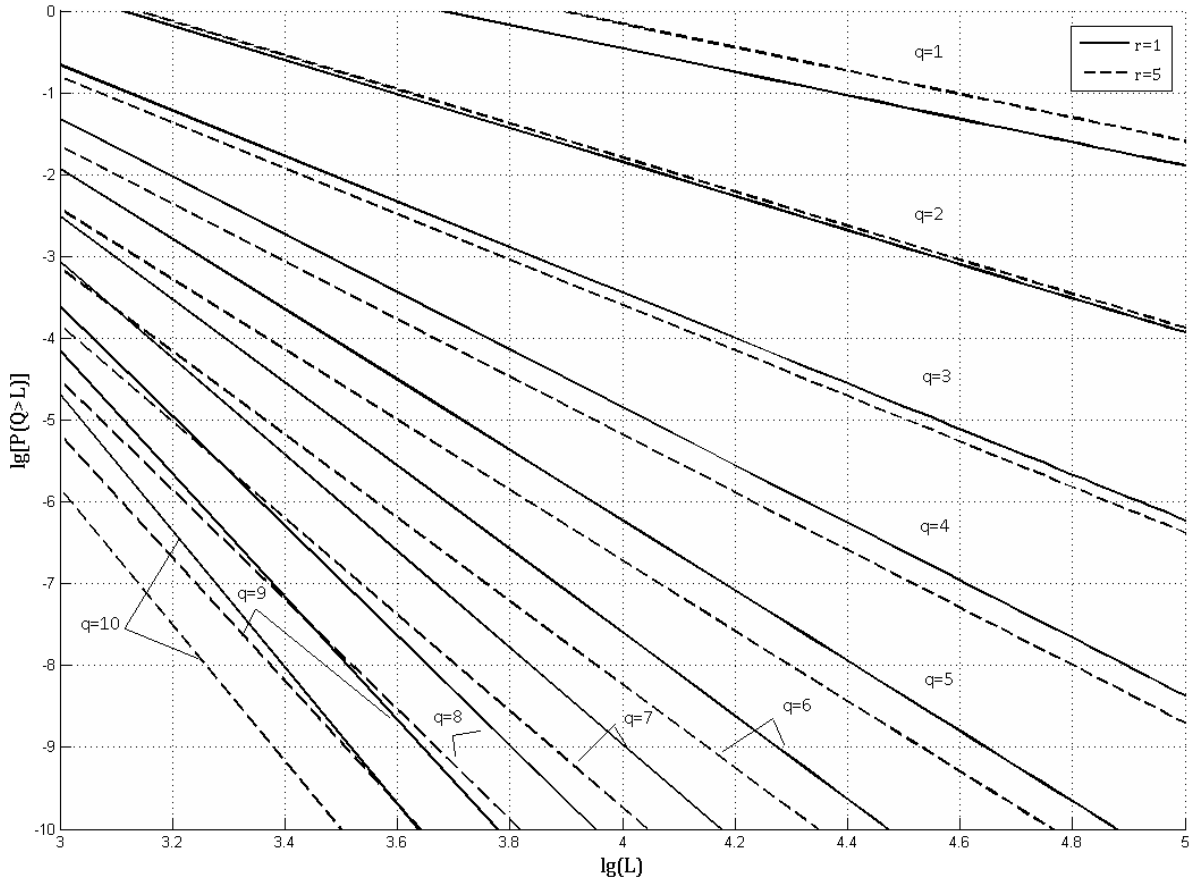

Box 2.

$$\log\left(P\left[Q > L\right]\right) \approx \min_{q>0} \log\left\{\sum_{i=0}^{3} c_i q^i + \tau_0\left(q\right)\log\left[\frac{b^{\,2\,\tau_0\left(q\right)}}{s\left(q-\tau_0\left(q\right)\right)}\right] - q\log\left[\frac{b^{\,2\,q}}{q-\tau_0\left(q\right)}\right]\right\} \quad (42)$$

where $\tau_0\left(q\right) = \sum_{i=0}^{3} a_i q + 1$

Figure 19. Dependences lnP[Q>L] from q at r =2 and r = 5

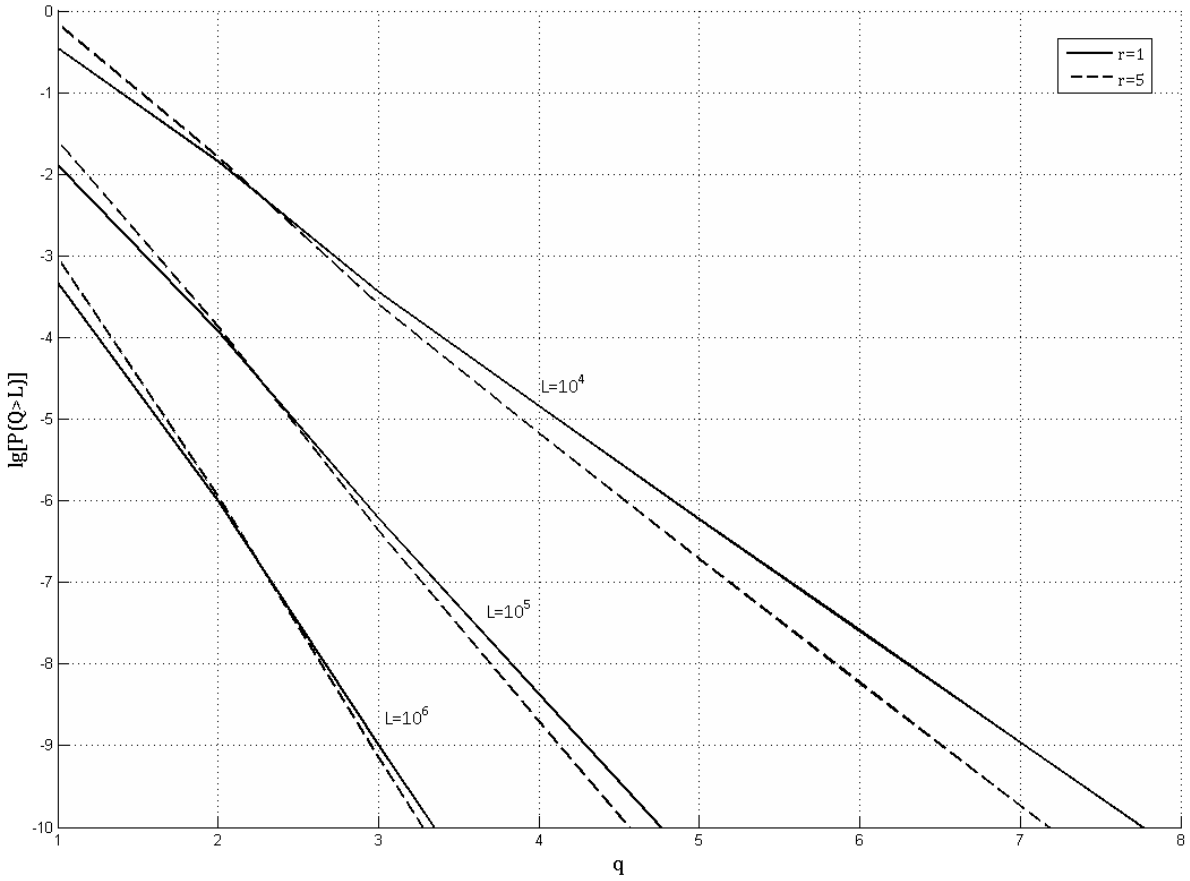

Function $\tau\left(q\right)$ can be considered as a scale-independent measure of a fractal signal. It is easy to connect it with *Renyi's dimensions*, *Hurst's* and *Holder parameters*. From expression (39) it is possible to calculate $\tau\left(q\right)$ using linear approximation. Subsequently, a multifractal spectrum $f(\alpha)$ can be found from the obtained value of $\tau\left(q\right)$. The functions $\tau\left(q\right)$ and $\log_2 c\left(q\right)$ found by nu-

multifractal traffic on an input of buffer device. It is shown that multifractal character of the traffic has essential impact on queuing performance characteristics. The greatest influence is caused by a component of the multifractal traffic with moment coefficient $q = 2$. With increasing q its impact on quality of service decreases. In actual use, it is sufficient to restrict the values of $q = 2 \ldots 5$.

REFERENCES

Bacry, E., Muzy, J. F., & Arneodo, A. (1993). Singularity spectrum of fractal signals: Exact results. *Journal of Statistical Physics*, *70*(3/4), 635–674. doi:10.1007/BF01053588.

Bozhokin, S. V., & Parshin, D. A. (2001). *Fractals and multifractals* [Regularnaya i haoticheskaya dinamika]. Izhevsk, Russia: NIC.

Brichet, F., Roberts, J., Simonian, A., & Veitch, D. (1996). Heavy traffic analysis of a storage model with long range dependent on/off sources. *Queueing Systems*, *23*, 197–215. doi:10.1007/BF01206557.

Dang, T. D. (2002). *New results in multifractal traffic analysis and modeling*. (Ph.D. Dissertation). Budapest, Hungary.

Feldmann, A., Gilbert, A. C., & Willinger, W. (1998). Data networks as cascades: Investigating the multifractal nature of internet WAN traffic. *ACM SIGCOMM Computer Communication Review*, *28*(4), 42–55. doi:10.1145/285243.285256.

Giordano, S., O'Connell, N., Pagano, M., & Procissi, G. (1999). A variational approach to the queuing analysis with fractional brownian motion input traffic. In *Proceedings of the 7th IFIP Workshop on Performance Modelling and Evaluation of ATM Networks*. Antwerp, Belgium: IFIP.

Hwang, W. L., & Mallat, S. (1994). Characterization of self-similar multifractals with wavelet maxima. *Journal of Applied and Computational Harmonic Analysis*, *1*, 316–328. doi:10.1006/acha.1994.1018.

Jaffard, S. (1997). Multifractal formalism for functions parts I and II. *SIAM Journal on Mathematical Analysis*, *28*(4), 944–998. doi:10.1137/S0036141095282991.

Lui, Z., Nain, P., Towsley, D., & Zhang, Z. L. (1999). Asymptotic behavior of a multiplexer fed by a long-range dependent process. *Journal of Applied Probability*, *36*, 105–118. doi:10.1239/jap/1032374233.

Mallat, S. (2005). *A wavelet tour of signal processing: The sparse way* (3rd ed.). New York: Academic Press.

Mandelbrot, B. (1982). *The fractal geometry of nature*. San Francisco, CA: Freeman.

Meyer, Y. (1997). *Wavelets, vibrations, and scalings*. Montreal, Canada: Universite de Montreal.

MIT Lincoln Laboratory. (2012). *1999 DARPA intrusion detection evaluation dataset*. Retrieved from http://www.ll.mit.edu/mission/communications/ist/corpora/ideval/data/index.html

Muzy, J. F., Bacry, E., & Arneodo, A. (1994). The muitifractal formalism revisited with wavelets. *International Journal of Bifurcation and Chaos in Applied Sciences and Engineering*, *4*, 245. doi:10.1142/S0218127494000204.

Muzy, J. F., Bacry, E., & Arneodo, A. (1999). Wavelets and multifractal formalism for singularity signals: Application to turbulence data. *Physical Review Letters*, *67*(25), 3515–3518. doi:10.1103/PhysRevLett.67.3515.

merical estimation can be approximated by the following types of polynomials:

$$\tau\left(q\right) = a_0 + a_1 q + a_2 q^2 + a_3 q^3 \quad (40)$$

and

$$\log_2 c\left(q\right) = c + cq + cq^2 + c_3 q^3 \quad (41)$$

Substituting into expression (36), we obtain formulas for estimating the probability of queue "tail" rejection with any kind of multifractal traffic on input (see Box 2).

NUMERICAL RESULTS

Consider the dataset taken from Internet traffic archive (MIT, 1999). The data structure is presented in Figure 16

The raw data was sampled at 1s intervals. The preliminary analysis of these implementations reveals their scaling properties; therefore they have been used as input process for the analysis of queuing performance. A plot of decomposition function of an investigated trace depending on decomposition level on *log-log* graph is shown in Figure 17 for some values of the q^{th} order moment.

Nonlinear scaling function $\tau\left(q\right)$ obtained according to the technique stated above is presented on Figure 17b, it reveals the scaling property of this dataset. After applying the estimation method stated above, functions $\tau_0\left(q\right)$ and $\log_2 c\left(q\right)$ have been calculated. The graph of function $\tau_0\left(q\right) = \tau\left(q\right) + 1$ is a convex curve; this speaks about the multifractal character of the investigated dataset. Parameters of a multifractal spectrum can be estimated from expression $f\ (\alpha) at\, q > 0,$ and are presented on Figure 2c. Approximation coefficients of functions $\tau\left(q\right)$ and $\log_2 c\left(q\right),$ corresponding to the resulting experimental data are presented in Table 2.

Substituting obtained values of approximation coefficients in expression (42), we obtain the analytical relationships illustrating efficiency of queue service in case of multifractal character of the processed traffic.

Figure 18 and 19 show the probability of exceeding the buffer length at an intensity of service $r = 2$ and $r = 5$ for the studied traffic with moment coefficient q taking values from 1 to 10. From these graphs it follows that the probability of dropping the "tail" for the traffic studied is much higher than the similar probability in the case of a fractional Brownian motion.

The conclusion, which follows from the presented relationships, is that the multifractal nature of traffic at the input buffer device has a significant influence on the characteristics of queuing. The largest component of the influence of multifractal traffic is observed for a moment coefficient value of $q = 2,$ with increasing q its impact on quality of service decreases. In actual use, it is sufficient to restrict the values of $q = 2\ ...5.$

CONCLUSION

For detection of traffic anomalies in computer and telecommunication networks the method based on multifractal data analysis at network layer is proposed. As the informative indicator, the use of distinction of fractal dimensions on various parts of a given dataset is introduced, and also parameters of a singularity spectrum estimated by means of Legendre transform.

A new method based on usage of multifractal spectrum parameters is proposed for the estimation of queuing performance for the generalized

Norros, I. (1994). A storage model with self-similar input. *Queueing Systems*, *16*, 387–396. doi:10.1007/BF01158964.

Park, K., & Willinger, W. (Eds.). (1999). *Self-similar network traffic and performance evaluation*. New York: Wiley-Interscience.

Riedi, R. H., Crouse, M. S., Ribeiro, V. J., & Baraniuk, R. G. (1999). A multifractal wavelet model with application to network traffic. *IEEE Transactions on Information Theory*, *45*(3). doi:10.1109/18.761337.

Shannon, C. E. (1948). A mathematical theory of communication. *The Bell System Technical Journal*, *27*, 379–423, 623–656.

Sheluhin, O. I., & Atayero, A. A. (2012). Detection of DoS and DDoS attacks in information communication networks with discrete wavelet analysis. *International Journal of Computer Science and Information Scurity*, *10*(1), 53–57.

Sheluhin, O. I., Atayero, A. A., & Garmashev, A. V. (2011). Detection of teletraffic anomalies using multifractal analysis. *International Journal of Advancements in Computing Technology*, *3*(4), 174–182. doi:10.4156/ijact.vol3.issue4.19.

Sheluhin, O. I., Smolskiy, S. M., & Osin, A. V. (2007). *Self-similar processes in telecommunications*. New York: John Wiley & Sons. doi:10.1002/9780470062098.

ADDITIONAL READING

Bakhoum & Toma. (2010). Mathematical transform of traveling-wave equations and phase aspects of quantum interaction. *Mathematical Problems in Engineering*. doi: doi:10.1155/2010/695208.

Beran. (1994). Statistics for long-memory processes. In *Monographs on Statistics and Applied Probability*. New York, NY: Chapmand and Hall.

Cattani & Kudreyko. (2008). On the discrete harmonic wavelet transform. *Mathematical Problems in Engineering*.

Cattani & Kudreyko. (2010). Application of periodized harmonic wavelets towards solution of eigenvalue problems for integral equations. *Mathematical Problems in Engineering*.

Cattani. (2009). Harmonic wavelet analysis of a localized fractal. *International Journal of Engineering and Interdisciplinary Mathematics, 1.*

Gong, Liu, Misra, & Towsley. (2005). Self-similarity and long range dependence on the internet: A second look at the evidence, origins, and implications. *Computer Networks*, *48*(3), 377–399. doi:10.1016/j.comnet.2004.11.026.

He & Leung. (2008). Network intrusion detection using CFAR abrupt-change detectors. *IEEE Transactions on Instrumentation and Measurement*, *57*(3), 490–497. doi:10.1109/TIM.2007.910108.

Leland, Taqqu, Willinger, & Wilson. (1994). On the self-similar nature of ethernet traffic. *IEEE/ACM Transactions on Networking*, *2*(1), 1–15. doi:10.1109/90.282603.

Li, Li, & Zhao. (2009). Experimental study of DDOS attacking of flood type based on NS2. *International Journal of Electronics and Computers*, *1*(2), 143–152.

Li & Lim. (2008). Modeling network traffic using generalized Cauchy process. *Physica A*, *387*(11), 2584–2594. doi:10.1016/j.physa.2008.01.026.

Li & Zhao. (2008). Detection of variations of local irregularity of traffic under DDOS flood attack. *Mathematical Problems in Engineering*.

Li & Zhao. (2010). Representation of a stochastic traffic bound. *IEEE Transactions on Parallel and Distributed Systems*, *21*(9), 1368–1372. doi:10.1109/TPDS.2009.162.

Li & Zhao. (2010). Variance bound of ACF estimation of one block of fGn with LRD. *Mathematical Problems in Engineering*.

Li. (2004). An approach to reliably identifying signs of DDOS flood attacks based on LRD traffic pattern recognition. *Computers and Security, 23*(7), 549–558.

Li. (2006). Change trend of averaged Hurst parameter of traffic under DDOS flood attacks. *Computers and Security, 25*(3), 213–220.

Li. (2010). Fractal time series: A tutorial review. *Mathematical Problems in Engineering.*

Paxson & Floyd. (1995). Wide area traffic: The failure of Poisson modeling. *IEEE/ACM Transactions on Networking*, *3*(3), 226–244. doi:10.1109/90.392383.

Rohani, M. Selamat, & Kettani (Eds.). (2008). *Proceedings from ICCCE '08: Continuous LoSS detection using iterative window based on SOSS model and MLS approach: International Conference on Computer and Communication Engineering*. Kuala Lumpur, Malaysia: ICCCE.

Sastry, Rawat, Pujari, & Gulati. (2007). Network traffic analysis using singular value decomposition and multiscale transforms. *Information Sciences*, *177*(23), 5275–5291. doi:10.1016/j.ins.2006.07.007.

Schleifer & Mannle. (2001). Online error detection through observation of traffic self-similarity. *IEE Proceedings. Communications*, *148*(1), 38–42. doi:10.1049/ip-com:20010063.

Sheluhin, & Atayero. (2012). Detection of DoS and DDoS attacks in information communication networks with discrete wavelet analysis. *International Journal of Computer Science and Information Security, 10*(1), 53-57.

Song, Ng, & Tang. (2004). Some results on the self-similarity property in communication\networks. *IEEE Transactions on Communications*, *52*(10), 1636–1642. doi:10.1109/TCOMM.2004.833136.

Tickoo & Sikdar. (2003). On the impact of IEEE 802.11 MAC on traffic characteristics. *IEEE Journal on Selected Areas in Communications*, *21*(2), 189–203. doi:10.1109/JSAC.2002.807346.

Toma. (2010). Specific differential equations for generating pulse sequences. *Mathematical Problems in Engineering*.

Wang & Yang. (2008). An intelligent method for real-time detection of DDoS attack based on fuzzy logic. *Journal of Electronics (China)*, *25*(4), 511–518. doi:10.1007/s11767-007-0056-6.